Critical behavior of the XY model in complex topologies

Miguel Ibáñez Berganza[*] and Luca Leuzzi[†]
IPCF-CNR, UOS Roma Kerberos and Dipartimento di Fisica, Università "La Sapienza", Piazzale A. Moro 5, 00185 Roma, Italy
(Received 26 November 2012; revised manuscript received 16 August 2013; published 15 October 2013)

The critical behavior of the $O(2)$ model on dilute Lévy graphs built on a two-dimensional square lattice is analyzed. Different qualitative cases are probed, varying the exponent ρ governing the dependence on the distance of the connectivity probability distribution. The mean-field regime, as well as the long-range and short-range non-mean-field regimes, are investigated by means of high-performance parallel Monte Carlo numerical simulations running on GPUs. The relationship between the long-range ρ exponent and the effective dimension of an equivalent short-range system with the same critical behavior is investigated. Evidence is provided for the effective short-range dimension to coincide with the spectral dimension of the Lévy graph for the XY model in the mean-field regime.

DOI: 10.1103/PhysRevB.88.144104 PACS number(s): 64.60.F−, 05.50.+q, 75.40.Mg, 64.60.aq

I. INTRODUCTION: INTERACTING MODELS IN COMPLEX NETWORKS

The study of interacting systems defined in complex, nonregular structures is interesting from at least two points of view. Statistical mechanical models in graphs are used for the description of phenomena in different fields, among which one can cite stock market dynamics,[1–4] correlations in bird flocking,[5] avalanches in brain activity,[6] or biological networks.[7,8] Furthermore, there is a theoretical interest *per se* in the study of criticality in complex networks. The theory of critical phenomena establishes that the critical properties of systems interacting in a d-dimensional lattice only depend on the symmetries of the interaction and on the dimensionality d. On the other hand, when the topology of the interaction is more complicated, e.g., translational invariance is lost and symmetries of the lattice are broken, the dependence of criticality on the structural properties of the interacting graph is not known in general, although this topic has been a subject of interest for more than two decades and several results are available for particular models.[9]

A particularly clear case is the spherical model, which has been proved to be equivalent to the $n \to \infty$ limit of the $O(n)$ model when both models are defined on a lattice.[10] On general graphs the full equivalence does not hold anymore, though the critical behavior of the spherical and $O(n \to \infty)$ still do coincide.[11] The critical properties of the spherical model on a general graph are exactly known[12] and are such that the universality class of the transition only depends on a single quantity: the spectral dimension of the graph, $\bar{d}$, defined in terms of the low-frequency spectral density of its adjacency matrix $\varrho(\omega) \sim \omega^{\bar{d}/2-1}$. This quantity is also related to the probability of self-return of a random walker in the graph, and determines the infrared divergences of a Gaussian field theory defined on the graph.[12,13] Remarkably, the functional dependence of the spherical model critical quantities on a graph with spectral dimension $\bar{d}$ turns out to be the same as that of a short-range model in a hyper-cubic lattice with Euclidean dimension $\bar{d}$. This analogy provides a suggestive, physical sense to the noninteger dimensions appearing in the context of the theory of critical phenomena.

The spectral dimension also plays a role in the XY model criticality, which was proved[14] to exhibit spontaneous magnetization in the ordered phase in a graph of spectral dimension $\bar{d} > 2$, and absence[15] of spontaneous magnetization for $\bar{d} \leqslant 2$. The latter phenomenon is well known in the two-dimensional (2d) XY model,[16–18] which is a particular case of this result.

Further numerical and analytical results for the criticality of other particular models in graphs are available (for a review see Ref. 9). The Ising model was first studied in small-world networks,[19–23] in Barabasi-Albert networks,[23–25] and on general graphs,[26,27] where it was found that the universality class depends on the divergence or finiteness of the second and fourth moments of the degree distribution. In this way, three different critical regimes may be discriminated: (i) absence of phase transition, when both second and fourth moments diverge; (ii) a non-mean-field second-order transition, when the second moment is finite; and (iii) a mean-field second-order transition, when both moments are finite.

Studies of the Ising model in scale-free networks[28] and in correlated growing-random networks[29,30] were also performed. In the latter case a phase transition was found of the Kosterlitz-Thouless (KT) universality class, different from the mean-field nature of the transition found in (uncorrelated) scale-free networks. This difference was argued to have its origin in the sign of the degree-degree correlations (assortativity-disassortativity) of both types of networks.[29,31] The Potts model has also been investigated,[32–34] finding an infinite-order transition for a divergent second moment of the degree distribution.

Eventually, also the $O(2)$ XY model has been analyzed. In the one-dimensional (1d) small-world network, it was argued[35] to exhibit long-range order for arbitrarily low values of the rewiring probability (like in the Ising case). For uncorrelated[4] and correlated[23] scale-free networks an order-disorder transition is observed for a sufficiently large value of the degree distribution exponent. Interestingly, as happens in the Ising case, in the correlated scale-free network the transition is non-mean-field, unlike the uncorrelated case. This difference is again ascribed to the different nature of the degree-degree correlations in both kinds of graphs.[4]

Another piece of the puzzle is provided by the numerical work carried out by Yang *et al.*,[36] in which the critical behavior of the XY model is studied in uncorrelated and correlated *random* (rather than scale-free) graphs. In the first case, i.e., the Erdös-Rényi graph, the transition is found to be of the mean-field type, while in a randomly growing network it is claimed that the occurring transition belongs to the KT universality class.

Despite numerous results in this field, a unified picture of critical phenomena in graphs is still lacking. For instance, it is not clear under what conditions a relation can be established between criticality in graphs with spectral dimension $\bar{d}$ and short-range models in $\bar{d}$ dimensional lattices, nor what is the relation with the conjectured influence of dissasortativity on criticality.

A. Lévy lattice

In order to study networks in different universality classes in a continuous way, and, thus, deepen the relationship between long-range system Euclidean dimension d, short-range equivalent Euclidean dimension D, and spectral dimension $\bar{d}$, we adopt the so-called *Lévy* or long-range *dilute* lattice.[37] It is a graph in which two nodes are connected with a probability decaying as a power ρ of their distance in a given d-dimensional lattice. The total number of links in the system is $Nz/2$, z being the average connectivity of a node. While for large enough ρ one recovers the d-dimensional hypercubic lattice, the $\rho = 0$ Lévy graph limit corresponds to the random Erdös-Rényi graph, such that the $zN/2$ bonds are chosen at random from the set of all $N(N-1)/2$ possible bonds. With respect to the fully connected version of the model, thus, the study of the model defined on the Lévy graph allows for more efficient computation, since the number of couplings grows only linearly with the size N. Varying the power ρ, one actually acts as if continuously varying the dimension of a D-dimensional short-range lattice model, equivalent—from the critical behavior point of view—to the long-range model.

The possibility yielded by Lévy lattices of changing the effective dimensionality, freely choosing the universality class of the model without compromising the computational complexity, is useful to approach different problems: the applicability of the replica symmetry breaking theory in and out of the spin-glass mean-field regime,[37,38] the existence of the Almeida-Thouless critical line above the spin-glass upper critical dimension in Ising[39,40] and Heisenberg[41] systems, the criticality of the 3-spin spin glass,[42] the random field Ising model transition at zero temperature,[43] and the low-temperature behavior in Heisenberg spin glasses (including the spin-chirality decoupling)[44,45] as well as in $O(m \to \infty)$ spin glasses.[46]

B. Criticality regimes

For fully connected systems with (ordered or disordered) long-range interactions decaying with the ρth power of the distance in a d-dimensional hypercubic lattice, three regimes can be identified:

(1) $d < \rho < \rho_{\rm mf}(d)$, in which the system undergoes a mean-field transition;

(2) $\rho_{\rm mf}(d) < \rho < \rho_{\rm sr}(d)$, in which infrared divergences take place, to be dealt with in the renormalization group approach;

(3) $\rho > \rho_{\rm sr}(d)$, where the critical behavior is short-range-like.

The value of $\rho_{\rm mf}(d)$ depends on the specific theory and its symmetries, thus being different in ordered[47] ($\rho_{\rm mf} = 3d/2$) and disordered (spin glass)[48] ($\rho_{\rm mf} = 4d/3$) systems. The exponent $\rho_{\rm sr}(d)$ is defined as the value of ρ at which long-range and short-range two-vertex functions display the same scaling behavior: $\rho_{\rm sr}(d) - d = 2 - \eta_{\rm sr}(d)$, where $\eta_{\rm sr}$ is the anomalous scaling exponent of the space correlation function in the D-dimensional short-range counterpart. The above scenario holds on the Lévy lattice, as well, where, besides, the mean-field regime is found also below $\rho = d$, down to $\rho = 0$.

Critical exponents are functions of ρ, as

$$\eta_\rho = 2 - \rho + d \tag{1}$$

for any ρ (the η long-range exponent is not renormalized) and

$$\nu_\rho = (\rho - d)^{-1} \tag{2}$$

valid only in the mean-field regime. These expressions are formally the same both in ordered systems[47] and in spin glasses,[48,49] whereas different is their dominion in ρ and the renormalized expression for $\rho > \rho_{\rm mf}(d)$. The prediction for the η_ρ exponent has been compared with the outcome of numerical simulations in the case of the long-range Ising ferromagnet.[50]

C. Short-range and long-range equivalence conjecture

Starting from the field-theoretic representation in the free theory limit, an equivalence between ρ and D can be conjectured:[37]

$$\begin{aligned} D &= \frac{2d}{\rho - d}\rho \in (d : 2+d], \\ D &= d \quad \rho \geqslant 2+d. \end{aligned} \tag{3}$$

This is exact up to $\rho = \rho_{\rm mf}$ (or down to $D = D_u$) but provides a $\rho_{\rm sr} = 2 + d$, which is wrong. It can be improved as[42,51]

$$D = \frac{2 - \eta_{\rm sr}(D)}{\rho - d} d \tag{4}$$

for which $D = d$ at the right $\rho_{\rm sr} = d + 2 - \eta_{\rm sr}(d)$. The above relationships hold in the absence of external fields and do not depend on the specific symmetries of the system, nor on the presence of any long-range order at all (as in the quenched disordered case). What changes is the range of values of ρ determining the universality class to which the model belongs.

So far Eq. (4) has been carefully tested in 1d Lévy Ising spin glasses for $\rho > \rho_{\rm mf}(1) = 4/3$, verifying that the equivalent short-range critical behaviors are actually consistent both for $D = 3$ ($\rho = 1.792$) and for $D = 4$ ($\rho = 1.58$). The compatibility is better the higher D ($D_u = 6$ in the spin-glass case).[51] In the 2d fully connected ordered Ising model at $\rho = 1.6546$ and 1.875, which, according to Eq. (4), should correspond to $D = 2$ and $D = 3$, respectively, numerical estimates of critical exponents are consistent nearer to the mean-field threshold (in $D = 3$) but for $\rho = 1.875$ they do not appear compatible anymore with the 2d model.[52] These observations hint that Eq. (4) is but an approximating interpolation beyond mean field. In the following we will test the conjectured relation Eq. (4) on the 2d XY model on Lévy graphs. To make reading more fluid and avoid notation ambiguities, in Table I we summarize various dimensions we refer to in this work.

TABLE I. Summary of the different dimensions considered.

d	Auxiliary lattice dimension
D	Critically equivalent short-range lattice dimension
$\bar{d}$	Lévy graph spectral dimension
D_u	Upper critical dimension

There are some aspects that should be clarified also in this context. An elementary question is about the relationship between the spectral dimension $\bar{d}$ of the graph and the short-range equivalent dimension D; cf. Eq. (3). A rigorous derivation of the critical properties of long-range dilute models as a function of the power ρ is still lacking, and also an argument stating under what conditions they are equivalent to the fully connected case with the same value of the power ρ. In what follows we will clarify some of the mentioned issues in the $O(2)$ case. Along with theoretical arguments, we shall present the outcome of numerical simulations run on graphics processing units (GPUs) with an *ad hoc* optimized code, whose dynamics is based on the Metropolis, parallel tempering, and overrelaxation algorithms, suited to study continuous spin models interacting in graphs with arbitrary topology (and possibly randomness).

The paper is organized as follows: In Sec. II we provide a theoretical argument to support the existence of three different universality classes of the $O(2)$ model defined on a dilute 2d graph with power ρ, relative to three intervals of the power ρ. We yield numerical evidence in support of the fact that in the mean-field regime the Euclidean $D(\rho)$ is, actually, the spectral dimension of the graph with power ρ. In Sec. III numerical methods are exposed. We present numerical results in Sec. IV and our conclusions in Sec. V.

II. CRITICALITY OF THE XY MODEL IN THE 2D LÉVY GRAPH

We are concerned with the ferromagnetic $O(n)$ model, defined by the Hamiltonian

$$H = -\sum_{i<j=1}^{N} J_{ij}\, \mathbf{S}_i \cdot \mathbf{S}_j, \tag{5}$$

where $\mathbf{S}_i$ denotes the dynamic variable on the ith site of the graph, an n-dimensional vector with unit modulus, and the product is a n-dimensional Euclidean scalar product, the XY model being the $n = 2$ case. The values of the adjacency matrix J_{ij} of the graph can be either 0 (no connection) or 1.

We will study the dilute Lévy graph, for which two sites i and j are connected (i.e., the element of the J_{ij} matrix is 1) with a probability

$$\mathcal{P}_\rho(J_{ij}) = \frac{1}{Z}|\mathbf{r}_i - \mathbf{r}_j|^{-\rho}, \qquad Z = \sum_r r^{-\rho}, \tag{6}$$

and such that the total number of bonds is independent from ρ and equal to $2N$ ($z = 4$, for periodic boundary conditions). In Eq. (6), the vector $\mathbf{r}_i$ corresponds to the position of site i on a square lattice and the probability is normalized summing over the set of all possible distances between the sites of the 2d lattice. Operatively, the set of possible distances on lattices of linear size L depends on the boundary conditions chosen for the numerical simulation being periodic (PBCs) or free (FBCs). The maximum distance $r_{\max}$ will be $[L/2]\sqrt{2}$ for PBCs or $L\sqrt{2}$ for FBCs.

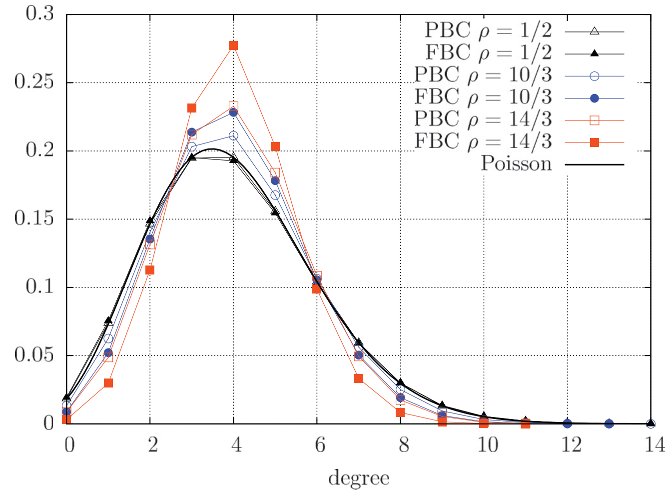

FIG. 1. (Color online) Probability distribution of the degree of connectivity of dilute 2d graphs with $N = 256^2$ nodes for three values of the decay exponent $\rho = 1/2, 10/3$ and $14/3$ of the link probability, one for each critical regime. Results are reported for both periodic (open symbols) and free (closed symbols) boundary conditions. $\rho = 14/3$ is in the short-range regime, $\rho = 10/3$ in the non-mean-field regime, and $\rho = 1/2$ in the mean-field regime. In the latter case the Poisson distribution with average 4 is displayed for comparison.

In Fig. 1 we show the degree distribution of the dilute 2d graph (with FBCs and PBCs) for different values of ρ. While the square lattice limit of the Lévy graph ($\rho \to \infty$) exhibits a delta function $\delta(z-4)$, the $\rho = 0$ limit corresponds to the Erdös-Rényi graph with degree distribution given by a Poisson distribution with average degree equal to 4. The latter case is independent from the kind of boundary conditions. The differences in the distribution of the number of connections per spin in systems with FBCs and with PBCs in the $\rho > 0$ case are finite-size effects that are stronger the larger ρ. Notwithstanding these differences, for what concerns universal quantities (i.e., critical exponents) the outcome of the numerical finite-size scaling (FSS) analysis of the critical behavior remains consistent when FBCs are implemented rather than PBCs, if the simulated sizes are large enough. We will show an instance of this consistency in Sec. IV. Unless otherwise stated, however, the results shown in the present paper are obtained from graphs with PBCs.

A. A dimensional argument

We now discuss the criticality of the model. Let us first consider the d-dimensional fully connected version of our model where each site is connected with any other site and the interaction strength decays with a power law $J(\mathbf{r}) \sim |r|^{-\rho}$ of the distance in a d-dimensional lattice. Following Ref. 47, we consider the following effective Ginzburg-Landau Hamiltonian for the long-range model, a scalar ϕ^4

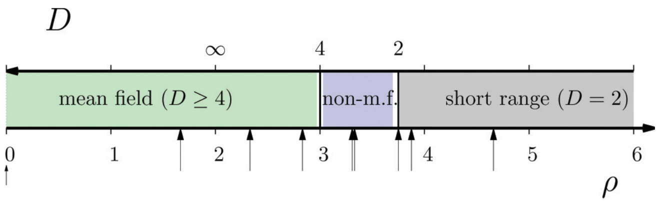

FIG. 2. (Color online) Three domains of ρ, relative to the three universality classes of the dilute *XY* model on the Lévy graph. The arrows point out at the values of ρ at which simulations have been carried out: 0, 1.667, 2.333, 2.833, 3.307933, 3.333, 3.75, 3.875, 4.67.

sine-Gordon theory,

$$\mathcal{H} = L^d \int \frac{d^d\mathbf{q}}{(2\pi)^d} (q^\psi + m^2) |\tilde{\phi}(\mathbf{q})|^2 + \frac{\lambda}{4!} \int d^d\mathbf{r}\, \phi^4(\mathbf{r}), \quad (7)$$

where L is the linear size of the system, $\mathbf{q}$ is the momentum space index, m is the mass of the theory, $\tilde{\phi}$ is the Fourier transform of the scalar field, and λ is the coupling strength. The long-range exponent ψ is such that the Fourier transform of the interaction $J(\mathbf{r})$ goes like

$$\tilde{J}(q) = L^{-d/2} \int d^d\mathbf{r}\, J(\mathbf{r}) e^{\imath \mathbf{r}\cdot\mathbf{q}} \sim q^{-\psi} \quad (8)$$

for low $q = |\mathbf{q}|$. In the long-range fully connected case ($J(\mathbf{r}) \sim r^{-\rho}$), it holds $\psi = \rho - d$, and there is a divergence for $\rho = d$, the point at which the number of links, proportional to $\tilde{J}(0)$, diverges in the thermodynamic limit.

A dimensional analysis of the Hamiltonian, Eq. (7), see, e.g., Refs. 37,47–49, shows that the dimension of the coupling constant λ is larger than zero whenever $\rho > 3d/2$. Below this point, λ is an irrelevant variable at criticality: the system critical behavior is correctly described by a (mean-field) free theory. For $\rho > \rho_{\rm sr}(d)$, the short-range lattice contribution to the propagator q^2 takes over the long-range q^ψ contribution and the Ginzburg-Landau Hamiltonian corresponds to the one of a d-dimensional short-range model. Considering the anomalous decay of the correlation function at criticality ψ has to be compared with $2 - \eta$ yielding $\rho_{\rm sr}(d) = 2 + d - \eta_{\rm sr}(d)$. We will motivate better in the following section such analogy (see also Sec. II B). Eventually, in the fully connected model, an ultraextensive regime occurs for $\rho < d$, with diverging energy. This is not present in the dilute model, since the number of bonds of the graph is constant. Collecting all the above considerations, we summarize the following dependence of the criticality of the dilute *XY* model on the exponent ρ (see Fig. 2):

(1) $\rho \geqslant \rho_{\rm sr}(d)$: The model should behave similarly to its short-range version in d dimensions, for what concerns criticality, thus belonging to the Kosterlitz-Thouless (KT) universality for $d = 2$. This regime will be called the *short-range (SR) regime* in the following.

(2) $\rho \in (\rho_{\rm mf}(d) : \rho_{\rm sr}(d))$, with $\rho_{\rm mf} = 3d/2$: The system will present a transition different from a KT transition, with exponents different from the mean-field ones; this regime will be denoted as the *long-range (LR) non-mean-field regime*.

(3) $\rho \leqslant \rho_{\rm mf}(d)$: The system belongs to the mean-field universality class; i.e., its critical properties are those corresponding to a free Gaussian theory in dimension 4. We will denote this regime as the *mean-field (MF) regime*.

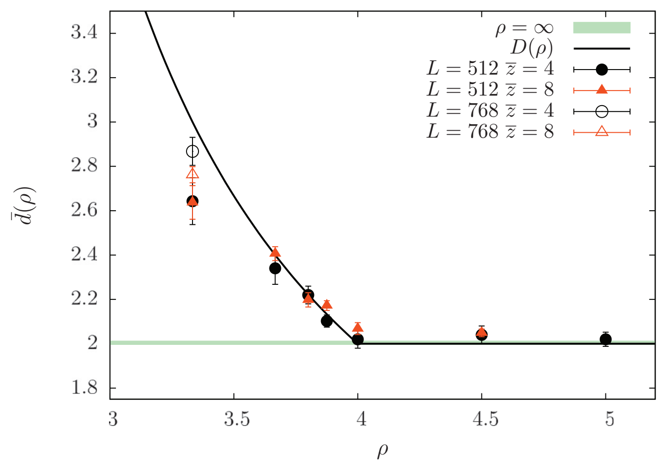

FIG. 3. (Color online) Spectral dimension $\bar{d}$, cf. Eq. (9), or equivalent short-range dimension $D(\rho)$, cf. Eq. (3), compared to the numerically estimated spectral dimension, versus ρ. The light full line is the result for the square lattice case $\rho = \infty$, the black full line is Eq. (9). The numerical estimate has been plotted for two sizes, $L = 512$ and 768 at the smaller $\rho = 10/3$, in order to highlight relevant finite-size effects when long-range connections occur. In all plotted cases, graphs with average connectivity $\bar{z} = 4$ and 8 have been considered.

B. Spectral dimension

Considering Eq. (3) one sees that the regimes above introduced are in correspondence with the three regimes of an *equivalent* D-dimensional lattice model with nearest-neighbor interactions: (1) short-range regime, $D = d$; (2) non-mean-field regime, $D \in (d : D_{\rm u})$; (3) mean-field regime, $D \geqslant D_{\rm u}$. Remarkably, this comparison suggests a tight relationship between D and the spectral dimension of the Lévy graph, $\bar{d}$. Indeed, in Ref. 53 it is proved that a fully connected lattice with interaction strength decaying as $r^{-\rho}$ (r being the distance in a d-dimensional lattice) has spectral dimension

$$\bar{d} = \begin{cases} d & \text{if} \quad \rho > 2 + d, \\ \frac{2d}{\rho - d} & \text{if} \quad \rho \in (d : 2 + d]. \end{cases} \quad (9)$$

It coincides with Eq. (3), holding in the mean-field regime $\rho \leqslant \rho_{\rm mf}(d) = 3d/2$. This implies that the relationship between critical properties of a model on a graph with spectral dimension $\bar{d}$ and on a lattice of Euclidean dimension $\bar{d}$, proved for spherical and $O(\infty)$ models,[12] still holds for the $O(2)$ model on Lévy lattice with $\rho \leqslant 3d/2$:

$$D = \bar{d}. \quad (10)$$

In the present section we provide an analysis of the spectral dimension directly supporting Eq. (9) also in dilute long-range random graphs. We numerically estimated the spectral dimension of 2d dilute Lévy graphs, with several values of the power ρ, through the calculation of the probability of self-return of a random walker in the graph after a time τ, $P(\tau)$, a quantity related[54] to the spectral dimension via

$$P(\tau) \sim \tau^{-\bar{d}/2} \quad (11)$$

for large τ. Our results are summarized in Fig. 3, in which we compare $\bar{d}(\rho)$ in Eq. (9) with the estimation of $\bar{d}$ at the corresponding ρ *via* the histogram of the random walker self-return times. As ρ decreases, finite-size effects become relevant, e.g., for $\rho = 10/3$. Details of the method are reported in Appendix A.

Figure 3 shows that the behavior of the spectral dimension is compatible with Eq. (9), even though strong finite-size effects take place as ρ decreases towards the mean-field threshold. To get an idea of finite-size effects, at $\rho = 10/3$ we present results obtained on graphs of linear size $L = 512$ and $L = 796$, with different average coordination number $\bar{z}$. We observe that $\bar{d}(10/3)$ increases towards the prediction of Eq. (9), $\bar{d} = 3$. This hints that the ρ dependence of the spectral dimension of the Lévy diluted 2d graph with power ρ coincides with the one of the fully connected version. Combined with Eq. (3), this also implies the equivalence between the spectral dimension of the graph $\bar{d}$ and the short-range dimension D of the XY model in the mean-field regime, $\rho \leqslant \rho_{\rm mf}(2) = 3$.

III. NUMERICAL METHOD, ALGORITHM, AND DETAILS OF THE SIMULATION

We now expose the numerical method used to analyze the critical properties of the XY model in dilute 2d lattices (5), via Monte Carlo sampling in finite-size realizations of graphs with N vertexes and $2N$ edges. Given T and ρ, we consider both the ensemble average $\langle \ldots \rangle$, at T, and the graph (topology) average $\overline{\quad}$ at ρ:

$$\overline{\langle O \rangle} = \frac{1}{\mathcal{Z}} \sum_{\{J\}} \sum_{\{\mathbf{S}\}} O\{\mathbf{S}\} \exp\left[-H\{\mathbf{S}\}/T\right] \mathcal{P}_\rho(J), \tag{12}$$

where H is the Hamiltonian of the model, Eq. (5), O is an observable, and $\mathcal{Z}$ is the partition function. The following quantities are measured: the specific heat

$$c = \frac{1}{N}\frac{\partial \overline{\langle H \rangle}}{\partial T} = \frac{1}{NT^2}\overline{(\langle H^2 \rangle - \langle H \rangle^2)}, \tag{13}$$

the susceptibility

$$\chi = N\overline{\langle \mathbf{m}^2 \rangle - \langle \mathbf{m} \rangle^2}, \tag{14}$$

and the fourth-order Binder cumulant

$$U_4 = \frac{\overline{\langle \mathbf{m}^4 \rangle}}{\overline{\langle \mathbf{m}^2 \rangle}^2} - 1, \tag{15}$$

where $\mathbf{m}$ is the magnetization,

$$\mathbf{m} = \frac{1}{N}\sum_{j=1}^{N} \mathbf{S}_j, \tag{16}$$

and where $\{\mathbf{S}_j\}_{j=1}^N$ is a given spin configuration. Yet another interesting scaling observable is the second-moment correlation length ξ:[55]

$$\xi = \frac{1}{2\sin(\mathbf{k}_{\min}/2)}\left[\frac{\chi(\mathbf{0})}{\chi(\mathbf{k}_{\min})} - 1\right]^{1/\psi}, \tag{17}$$

where $\psi = \rho - d$ in the long-range regime and $\psi = 2$ in the short-range regime, cf. Eqs. (7) and (8), $\mathbf{k}_{\min} = (2\pi/L,0) = (0,2\pi/L)$ is the smallest momentum in the Fourier space, and $\chi(\mathbf{k})$ is the Fourier transform of the equilibrium two-point correlation function

$$C(\mathbf{r}) = \frac{1}{N}\sum_{\mathbf{i}} \overline{\langle \mathbf{S_i} \cdot \mathbf{S_{i+r}} \rangle}. \tag{18}$$

With these observables we analyze the critical properties of the model around the critical temperature T_c using the scaling relations

$$U_4(T,N) = \tilde{U}_4(t\, N^{1/\bar{\nu}}); \tag{19}$$

$$c(T,N) = \begin{cases} N^{\alpha/\bar{\nu}}\, \tilde{c}(t\, N^{1/\bar{\nu}}), & \rho > \rho_{\rm mf}, \\ \tilde{c}(t\, N^{1/2}), & \rho \leqslant \rho_{\rm mf}; \end{cases} \tag{20}$$

$$\chi(T,N) = \begin{cases} N^{\gamma/\bar{\nu}}\, \tilde{\chi}(t\, N^{1/\bar{\nu}}), & \rho > \rho_{\rm mf}, \\ N^{1/2}\, \tilde{\chi}(t\, N^{1/2}), & \rho \leqslant \rho_{\rm mf}; \end{cases} \tag{21}$$

$$\xi(T,N) = \begin{cases} L\tilde{\xi}(t\, L^{1/\nu_\rho}), & \rho > \rho_{\rm mf}, \\ L^{1/\psi}\tilde{\xi}(t\, N^{1/2}), & d < \rho \leqslant \rho_{\rm mf}; \end{cases} \tag{22}$$

where $t = T - T_c$, α and γ are the standard critical exponents, and $\bar{\nu}$ is the correlation volume exponent. This is suited to study scaling relations in graphs and fully connected systems,[35,56] in which the correlation length is no longer well defined, but for which the correlation volume V diverges at the critical point as $V \sim t^{-\bar{\nu}}$. The correlation volume exponent is related to the correlation length exponent of the short-range equivalent system by

$$\bar{\nu} \equiv \begin{cases} D\nu_{\rm sr}(D) & D < D_u, \\ D_u \nu_{\rm sr}^{\rm mf} = 2 & D \geqslant D_u. \end{cases} \tag{23}$$

According to the conjectured LR-SR equivalence in free energy density scaling,[51] $\nu_{\rm sr}(D)D = \nu_\rho(d)d$, one can hypothesize the following relationship to the LR exponents:

$$\bar{\nu} = \begin{cases} d\nu_\rho(d) & \rho > \rho_{\rm mf}(d), \\ d\nu_{\rho_{\rm mf}}(d) = 2 & \rho \leqslant \rho_{\rm mf}(d) = \frac{3}{2}d. \end{cases} \tag{24}$$

Consequently, using the Widom scaling relation

$$\frac{\gamma}{\nu_\rho} = 2 - \eta_\rho, \tag{25}$$

one has

$$\frac{\gamma}{\bar{\nu}} = \frac{\gamma}{d\nu_\rho} = \begin{cases} \rho/d - 1 & \rho > \rho_{\rm mf}(d), \\ 1/2 & \rho \leqslant \rho_{\rm mf}(d) = \frac{3}{2}d, \end{cases} \tag{26}$$

which can be easily verified/falsified, thus yielding information about the reliability of the SR-LR equivalence.

IV. NUMERICAL RESULTS

According to the arguments of Sec. II, and in order to elucidate the nature of the phase transition in each regime, we have run various sets of simulation with the values of ρ reported in the first column of Table II, cf. Fig. 2, $\rho = 0$, 1.667, 2.333, 2.833, 3.307933, 3.333, 3.75, 3.875, 4.667, and on the 2d square lattice, corresponding to $\rho = \infty$. We have studied finite-size realizations of the system in Lévy graphs with $N = L^2$, $L = 16, 32, 64, 128, 256, 384$ nodes. Each run, for a fixed topology, consists of 2^{21} Monte Carlo steps (MCSs). We measure observables each every MCSs. Time averages are

TABLE II. Estimations of the critical temperature and of the $\bar{\nu}$, γ, β, and η exponents for various values of ρ.

	0	5/3	7/3	17/6	3.307933	10/3	3.75	3.875	14/3	∞
T_c from T_f	1.93(1)	1.96(1)	1.94(1)	2.01(1)	1.76(1)	1.75(2)	1.63(1)	1.58(1)	1.36(1)	0.89(1)
T_c from U crosses	1.93(1)	1.96(1)	1.94(1)	2.00(1)	1.76(1)	1.75(2)	1.62(2)	1.57(1)	1.38(2)	
T_c from KT law								1.59(1)	1.34(2)	0.893(4)
T_c from η FSS							1.60(2)	1.56(1)	1.37(1)	0.894(5)
$\bar{\nu}$	2.00(2)	2.00(3)	2.00(3)	2.00(2)	2.18(2)	2.19(2)	2.40(3)			
γ	1.00(1)	1.00(4)	0.99(6)	0.97(4)	1.42(7)	1.45(5)	2.10(4)			
$\beta/\bar{\nu}$	0.25(1)	0.25(1)	0.26(2)	0.25(2)	0.178(6)	0.15(2)				
η							0.25(2)	0.25(1)	0.26(2)	0.250(1)

performed on exponentially increasing windows (between 2^k and 2^{k+1}, $k = 1,\ldots,19,20$). Topology averages are performed over a sampling of N_g simulations with different realizations of the graph topology, with N_g decreasing for increasing N: $N_g = 160$ for $L = 16,\ldots,128$, $N_g = 6$ for $L = 256$, $N_g = 4$ for $L = 384$. Equilibration checks have been done by comparing time averages of observables on exponentially increasing time windows and verifying the consistency of the energy and magnetization histograms and the correlation length values for the last two time windows. As a further equilibration test, we have checked the coincidence of specific heat measurements according to the equality in Eq. (13). The algorithm used, a parallel exchange Monte Carlo with overrelaxation implemented on GPUs, is described in detail in Appendix B.

In this section we present numerical results supporting the considerations about the XY model criticality as a function of ρ that we presented in Sec. II. As reference for the rest of the paper, results for the critical behavior are summarized in Figs. 4, 5, 6 and in Table II. We now proceed to analyze and discuss the critical behavior in the different regimes, starting with the two extreme model limits: the 2d and the Erdos-Renyi XY models.

A. Kosterlitz-Thouless transition: 2d square lattice limit

As a benchmark test we have analyzed the outcome of our algorithm in the square lattice (the $\rho = \infty$ limit), where the XY model is known to undergo an infinitely high order transition, the KT transition.[16,17] The paramagnetic high-temperature phase, in which vortices are *unbound*, displays exponentially decaying spatial correlations. The low-temperature spin-wave phase is made of coupled pairs of vortices of opposite chirality. It is characterized by the absence of spontaneous magnetization and a power-law asymptotic decay of the spatial correlation function.

We can compare our results with the analysis of Ref. 58, finding excellent agreement for all the analyzed quantities (χ, $\langle H\rangle$, ξ, c). Looking at the FSS of the temperatures relative to fixed values of the Binder cumulant, we find $T_c = 0.89(1)$. We also find $T_c = 0.894(5)$ with an independent estimate (see below). As a further test, we have looked at several properties of the KT transition, which we will also consider as fingerprints for the classification that we will do in the following; cf. Sec. IV E. We enumerate them for clarity:

(1) *Scale invariance in the whole range* $T \leqslant T_c$. The scaling functions ξ/L and U_4 are scale invariant for all $T < T_c$ in the large-N limit.[59] Differently from what happens, for example, in standard second-order phase transitions, one observes a

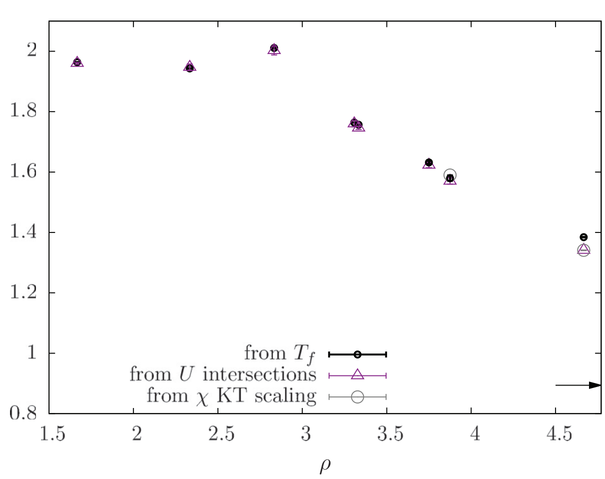

FIG. 4. (Color online) Critical temperature in the MF, LR, and SR regimes, according to the two different estimation methods described in Appendix C and to the $N \to \infty$ extrapolation of the critical temperatures from the KT scaling (29). The horizontal arrow marks the position of the 2d critical temperature.

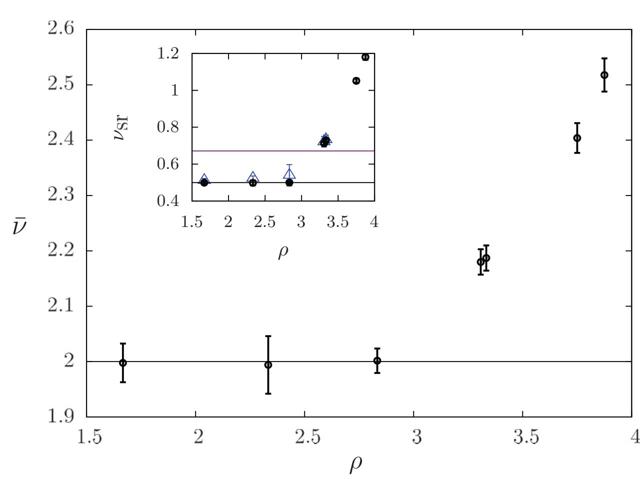

FIG. 5. (Color online) Correlation volume exponent $\bar{\nu}$ vs ρ. Inset: $\nu = \bar{\nu}/D(\rho)$ with $D(\rho)$ given by (3). The horizontal lines are the mean-field value, 1/2, and the value corresponding to the 3d XY model (Ref. 57): $\nu_{3d} = 0.6717(1)$. The blue triangles are the results of an apart analysis [x^{-1} from Eq. (C1)]; cf. Appendix C.

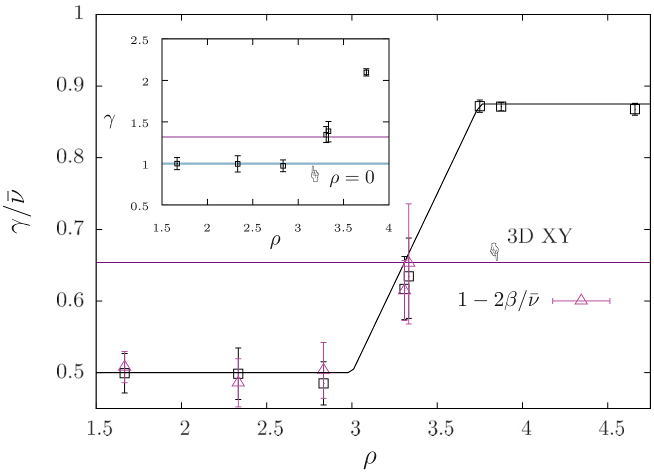

FIG. 6. (Color online) Estimations of $\gamma/\bar{\nu}$ (squares) and of $1-2\beta/\bar{\nu}$ (triangles). The horizontal line indicates the value of $\gamma_{3d}/3\nu_{3d}$ (Ref. 57), while the black curve is Eq. (26). For $3<\rho<4$, the points indicate the average of two values of $\gamma/\bar{\nu}$ corresponding to two temperatures in the error interval of the estimated critical temperature: $T=1.75$ and $T=1.76$ for $\rho=3.307933$ and $T=1.744$ and 1.75 for $\rho=10/3$. The inset shows the value of γ obtained multiplying the estimation of $\gamma/\bar{\nu}$ by the estimation of $\bar{\nu}$ in Fig. 5. The magenta horizontal line indicates γ_{3d}, while the green horizontal stripe stands for the estimation of the $\rho=0$ case.

superposition of the finite-size ξ/L curves corresponding to different, sufficiently large, values of L (see Fig. 9, right panel). In particular, this does not allow us to infer the critical temperature from the FSS of crossing points of U_4 or ξ/L. We can, however, estimate T_c by means of the fixed U_4 FSS method described in Appendix C, yielding $T_c = 0.89(1)$.

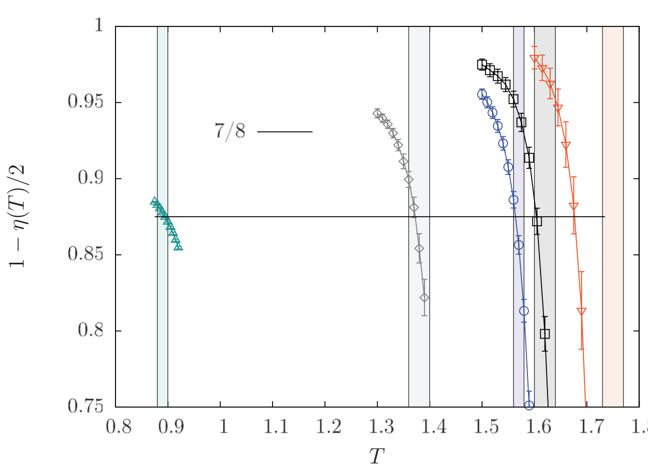

FIG. 7. (Color online) The critical exponent $1-\eta/2$ versus temperature for—from left to right—the 2d model, $\rho=4.667, 3.875$, $\rho_{sr}=3.75$, and $\rho=3.333$, the latter being in the LR regime. The horizontal line is the value in the SR universality class. The vertical bars are the estimates of the critical temperature for the different cases with their error bars. In all the cases with $\rho \geqslant 3.75$ the SR critical value of the η exponent is compatible with our independent estimates of the critical point. In the latter case, not belonging to the SR universality class, this is clearly not occurring.

(2) *Susceptibility scaling at criticality.* The susceptibility Eq. (14) at $T=T_c$ is predicted to behave like

$$\chi \propto L^{2-\eta}(\ln L)^{-2r} \tag{27}$$

with $\eta = 1/4$ and $r=1/16$.[60] Numerically interpolating Eq. (27) at different temperatures we found that the temperature at which $\eta=1/4$ is compatible, in the statistical error, with our estimate for T_c. In Fig. 7 (leftmost curve) we plot $1-\eta(T)/2$ as estimated in this way. It can be graphically seen that the KT value at criticality is, indeed, reached in the right T_c interval. We can, vice-versa, interpolate a value of T_c as the temperature at which $\eta(T_c)=1/4$, yielding $T_c=0.894(5)$ with our data, in agreement with recent very precise simulations.[61]

(3) *Absence of magnetization in the low-T phase*. We find numerical evidence of vanishing magnetization in the cold phase by looking at the FSS of $\langle \mathbf{m}^2\rangle$, or, more precisely, at $\chi/N = \langle \mathbf{m}^2\rangle - \langle \mathbf{m}\rangle^2$. The latter term $\langle \mathbf{m}\rangle^2$ is numerically not strictly zero but turns out to be always much smaller than $\langle \mathbf{m}^2\rangle$ below the critical point and tends to decrease for the largest sizes. The FSS behavior of χ and $\langle \mathbf{m}^2\rangle$ below criticality thus turns out to be practically identical at the leading term:

$$\sqrt{\langle \mathbf{m}^2\rangle} \simeq \sqrt{\chi/N} = \text{const}\, N^{-\eta/4}. \tag{28}$$

We verified the goodness of this interpolation tending to zero for $N\to\infty$, compatibly with the observation of zero magnetization[61] characteristic of the KT transition. We notice that the dependence in N is very slow because $\eta/4 = 1/16$ in the short-range universality class.

(4) *Continuous specific heat at the transition*, as can be seen in Fig. 8.

(5) *Exponential divergence: Kosterlitz-Thouless law*. Susceptibility and correlation length behave at criticality according to the law[17]

$$X = X_0 \exp\left\{\frac{b_X}{\sqrt{T-T_X}}\right\} \tag{29}$$

with $X=\xi,\chi$. Figure 9 illustrates FS behavior of χ and ξ. As the size increases the behavior tends to Eq. (29) for a larger

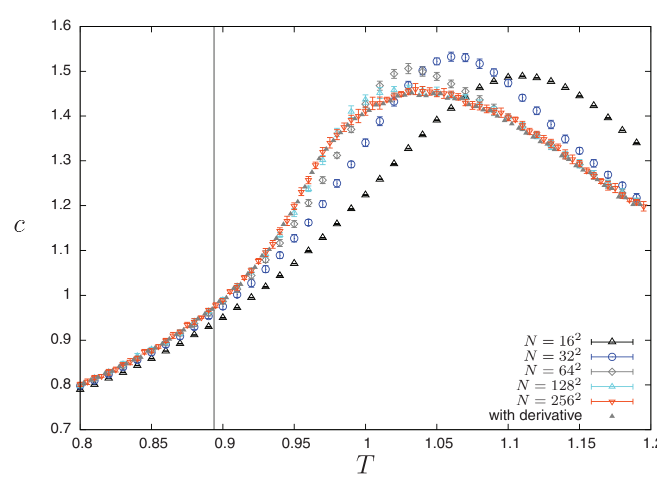

FIG. 8. (Color online) Specific heat versus temperature for the 2d system in lattices of size $N=2^{2n}$, $n=4,\ldots,8$. The vertical line indicates the estimated value of the critical temperature.

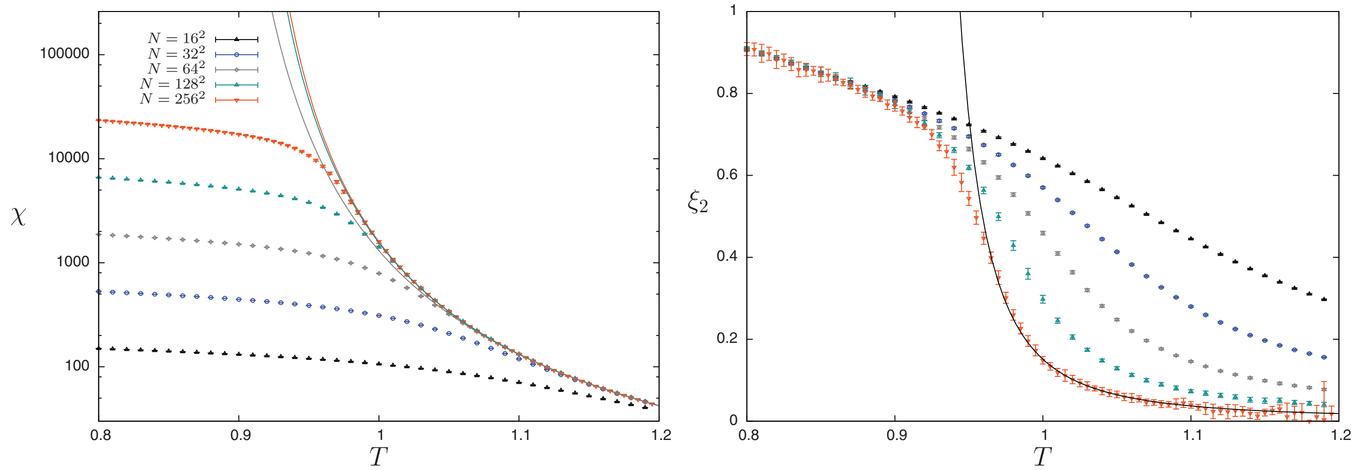

FIG. 9. (Color online) Magnetic susceptibility (left) and correlation length (right) of the 2d model vs T. As N increases, $\chi(T)$ becomes more and more similar to the functional law Eq. (29). In the low-temperature phase the ξ curves collapse onto each other.

interval of temperature. Interpolating $\chi(T,N)$ with Eq. (29) at fixed N with data in the high-T phase we obtain different size-dependent curves with parameters $\chi_0(N)$, $b_\chi(N)$, and $T_\chi(N)$. A further estimate of the critical temperature may then be obtained by extrapolating $T_c = T_\chi(\infty)$ with the law $T_\chi(N) = T_\chi(\infty) + \text{const}\, N^{-3/2}$. With such a method we obtain the critical temperature $T_c = 0.893(4)$, compatible with the other estimates.

B. Erdös-Rényi limit

As a further check we have studied the $\rho = 0$ limit, corresponding to a random Erdös-Rényi graph with a Poisson distribution of the degree of connectivity and average degree equal to 4. We report numerical evidence for a second-order mean-field phase transition. Our results are compatible with the theoretical values of the critical exponents $\bar{\nu} = 2$, $\gamma = 1$, and $\alpha = 0$, as argued in Sec. II, and are in agreement with the numerical estimates of Refs. 35,36, where the mean-field transition on Erdös-Rényi graphs of average degree 3 and 8, respectively, have been analyzed.

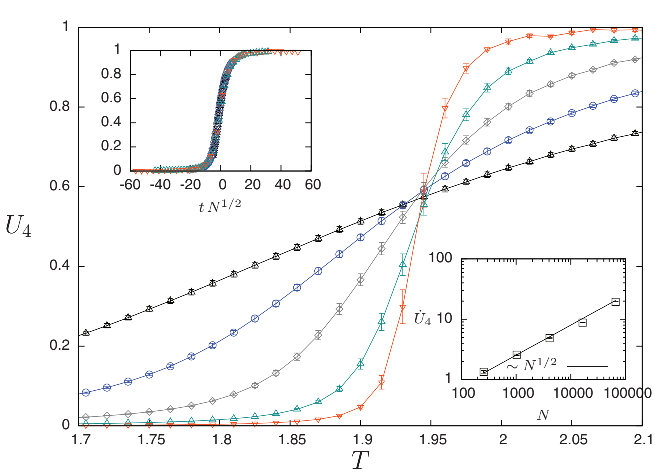

FIG. 10. (Color online) Binder cumulant versus temperature for $\rho = 2.333$ in the mean-field regime. The upper inset shows the scaling (19) with $\bar{\nu} = 2.00(3)$ and the lower inset is the calculation of $\bar{\nu}$ with the relation (30).

As in the previous subsection, we now present the salient analysis for the Erdös-Rényi case. The critical temperature is estimated from the FSS of the value $T(N)$ at which the cumulant $U_4(T,N)$ intersects with $U_4(T,N/4)$. Assuming the FSS $T(N) = CN^{-1/\bar{\nu}} + T_c$, we obtain $T_c = 1.93(1)$, in agreement with the analytic value $T_c = 1.9361$.[62] This is also the point at which the specific heat curves for different sizes cross each other, according to the scaling law Eq. (20).

The exponent $\bar{\nu}$ may be estimated by interpolating the relation

$$\left.\frac{\partial U_4(T,N)}{\partial T}\right|_{U_4=\text{const}} \sim N^{1/\bar{\nu}}, \tag{30}$$

where the derivative of U_4 with respect to the temperature is evaluated at fixed values of U_4 in the scaling critical region, yielding $\bar{\nu} = 2.00(2)$, in agreement with the mean-field value $\bar{\nu} = 2$. Further numerical estimates for the mean-field critical exponents may be found in the rescaling of the functions χ and U_4 as shown for qualitatively similar mean-field cases (see later). We remark that, although the values of the critical exponents are the mean field ones, the value of the critical temperature is not a universal quantity and does not coincide with the Gaussian mean-field value[13] $T = 2$.

We also checked the Rushbrooke scaling relation $2\beta + \gamma = 2 - \alpha$ by observing the right scaling of the magnetization with the mean-field exponent $\beta = 1/2$. Indeed, an important feature of this mean-field transition is that the low-temperature phase presents a finite magnetization, and this is confirmed by FSS analysis of $\overline{\langle \mathbf{m}^2 \rangle}$ in the low-T phase.

C. Long-range mean-field regime

We repeated the same analysis for $\rho = 5/3, 7/3$, and $17/6$, in the mean-field regime. The first value is nearer to the limit of convergence ($\rho = d = 2$) of the fully connected model, where the largest differences with the dilute model could possibly arise. The last value of ρ is very near the mean-field threshold $\rho_{\rm mf} = 3d/2 = 3$. Through FSS of the Binder cumulant we

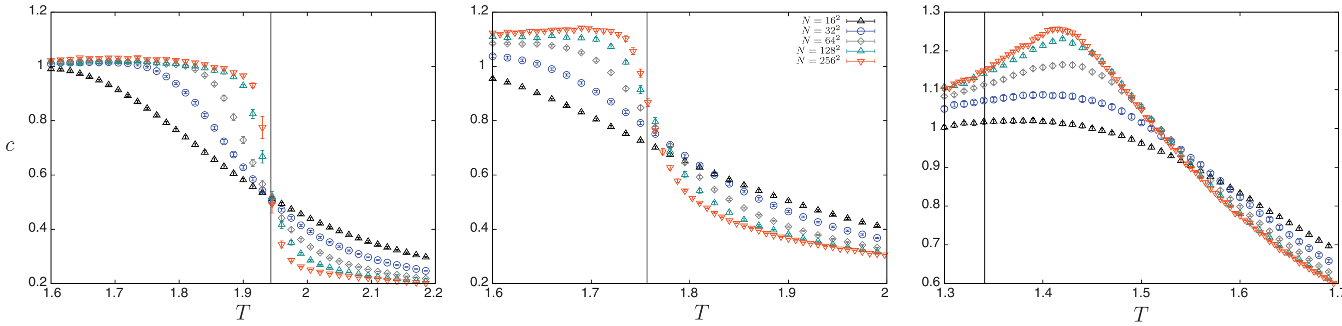

FIG. 11. (Color online) Specific heat versus temperature for different Lévy lattices. Left: Dilute model with $\rho = 7/3$ in the mean-field regime. Center: Dilute model with $\rho = 10/3$ in the non-mean-field long-range regime. Right: Dilute model with $\rho = 14/3$ in the short-range regime. In the last case the large-N limit of c is regular and continuous at any T.

estimate $T_c = 1.96(1), 1.94(1)$, and $2.01(1)$, respectively. In Fig. 10 we show the Binder cumulant and its scaling for $\rho = 7/3$. The derivative of U_4 with respect to T allows us to estimate $\bar{\nu} = 2.00(3), 2.00(3)$, and $2.00(2)$, respectively. These are all compatible with mean-field theory; cf. Eqs. (23) and (24).

From the data reported in Fig. 11, left panel, one observes a scaling of the type $c(T,N) = \tilde{c}(t\, N^{1/2})$, suggesting that $\alpha = 0$. We checked the $\gamma = \bar{\nu}/2$ mean-field scaling relation for the exponents by fitting the function $\ln \chi(T,N) = \gamma/\bar{\nu} \ln N + \ln \tilde{\chi}(\tilde{t})$ as a function of $\ln N$ for fixed values of $\tilde{t}$ in the scaling regime obtaining $\gamma = 1.00(4), 0.99(6)$, and $0.97(4)$, respectively. The rescaled χ curve for $\rho = 7/3$ is plotted in Fig. 12, left panel.

Finally, one finds that there is spontaneous magnetization in the low-temperature phase. The size dependence of the square root of $\overline{\langle \mathbf{m}^2 \rangle}$ is very poor and practically no finite-size scaling is observed at the largest simulated sizes. In Fig. 13 the plot for $\rho = 7/3$ is shown (left panel).

These numerical results strongly hint that the system belongs to the mean-field universality class in the range $\rho \in [0{:}3]$. In the whole range the critical exponents are well defined and estimated.

D. Long-range non-mean-field regime

An analogous investigation leads to a different behavior in the non-mean-field regime, for $3 < \rho < 3.75$. We simulated systems at $\rho = 3.3079$ and 3.3333. The critical temperature estimates obtained from the U_4 crossing points (cf. Fig. 14 for $\rho = 3.3333$) are, respectively, $T_c = 1.76(1)$ and $1.75(2)$. The FSS analysis of Eq. (30) reveals a correlation volume exponent larger that the mean-field value 2 and increasing with ρ: $\bar{\nu} = 2.18(2)$ and $2.19(2)$.

In Fig. 14, next to the main plot, we show in the insets the U_4 rescaling at $\rho = 10/3$ both for lattices with periodic and free boundary conditions. In the latter case $T_c = 1.53(2)$ and $\bar{\nu} = 2.20(3)$, the exponent being consistent with the FSS value from lattices with PBC. Also the susceptibility exponent turns out to be larger than its mean-field value, respectively, $\gamma = 1.42(7)$ and $1.45(5)$. We, further, observe a low-T magnetized state, $\overline{\langle \mathbf{m}^2 \rangle} \neq 0$, almost insensitive to size, as in the mean-field case; cf. Fig. 15.

Comparison with three-dimensional critical exponents. In Figs. 5 and 6 we also compare the values of the ν and γ exponents at $\rho = 3.307933$ [for which the equivalent short-range dimension is $D = 3$ according to Eq. (4)] with their

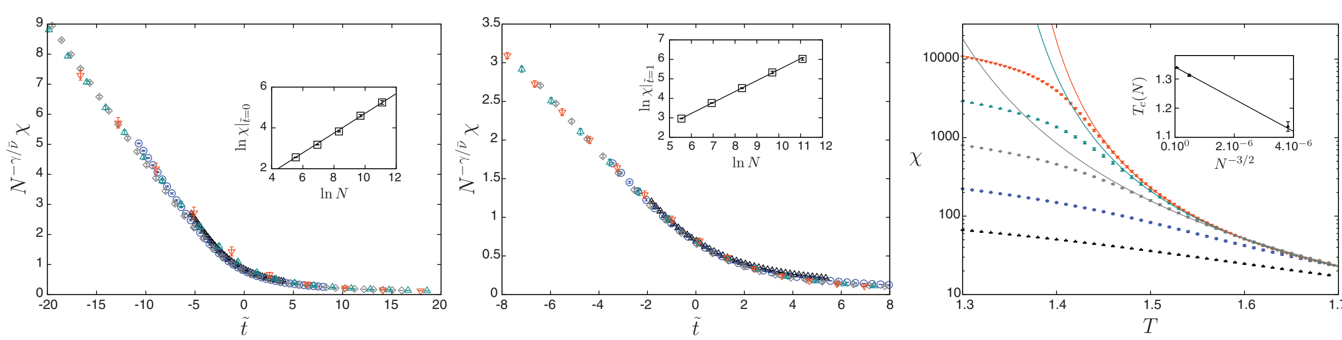

FIG. 12. (Color online) Magnetic susceptibility versus T for different Lévy graphs Left: Susceptibility scaling, according to Eq. (19), in the mean-field regime, $\rho = 7/3$, $T_c = 1.94(1)$, $\bar{\nu} = 2.00(3)$. Inset: Finite-size behavior of $\ln \chi$ at fixed $\tilde{t}$, yielding $\gamma = 0.99(6)$. Center: Susceptibility scaling for $\rho = 10/3$, in the non-mean-field long-range regime; $T_c = 1.75(2)$, $\bar{\nu} = 2.19(2)$. Inset: FSS of $\ln \chi$ at fixed $\tilde{t}$, yielding $\gamma = 1.45(5)$. Right: Susceptibility vs temperature for the Lévy short-range case $\rho = 14/3$. As the size increases, $\chi(T)$ becomes more and more similar to the functional law Eq. (29), with which we fitted the data of the systems of size $N = 64^2, 128^2$, and 256^2 in a temperature interval beginning at $T = 1.48$, 1.47, 1.45, respectively. The N dependence of the so obtained T_c is shown in the inset, together with the fit which extrapolates to $N = \infty$.

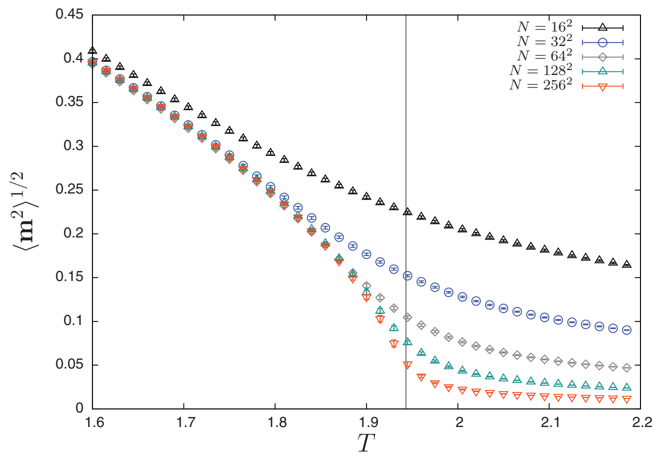

FIG. 13. (Color online) Square root of the average squared magnetization versus temperature for $\rho = 2.333$, in the mean-field regime. As N increases, the low-temperature phase exhibits finite spontaneous magnetization.

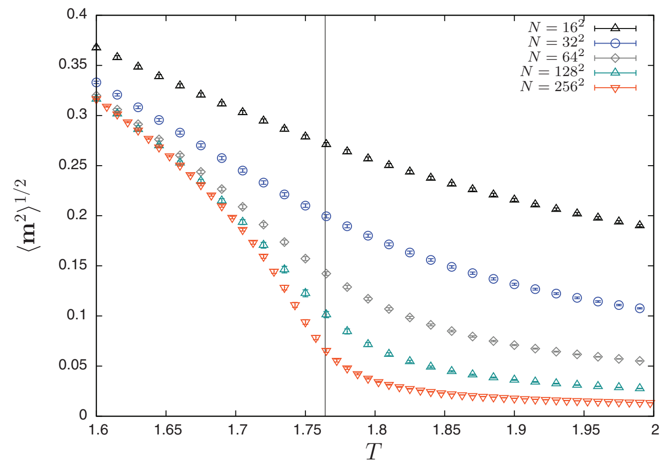

FIG. 15. (Color online) Square root of the average squared magnetization versus temperature for $\rho = 10/3$ (right), in the non-mean-field long-range regime. As N increases, the low-temperature phase exhibits finite spontaneous magnetization.

value in the three-dimensional (3d) XY model, obtained from a state-of-the-art numerical analysis.[57]

In particular, for $\rho = 3.307933$, we find $\gamma = 1.42(7)$, $\bar{\nu} = 2.18(2)$, $\beta = 0.39(2)$ to be compared with the values $\gamma_{3\mathrm{d}} = 1.3178(2)$, $\bar{\nu}_{3\mathrm{d}} = 3\nu_{3\mathrm{d}} = 2.0151(3)$, $\beta_{3\mathrm{d}} = 0.3486(1)$. Apparently, apart from γ displaying the largest statistical uncertainty, these values do not satisfy the quantitative relationships following the LR-SR equivalence conjecture, cf. Eq. (4) and Eq. (24), even though their difference is rather small (a few percent), as can be appreciated looking at Figs. 5 and 6. The lack of accuracy in the determination of γ comes from the fact that it is very sensitive to the value of the critical temperature used (see Appendix C). The comparison is not any better choosing $\rho = 10/3$ corresponding to a spectral, rather than Euclidean, dimension $\bar{d} = 3$.

E. Short-range regime

The cases $\rho = 3.75, 3.875$, and 4.667 have been simulated and analyzed finding evidence that they belong to the KT universality class of the 2d short-range XY model. They also display some peculiar features that we compare to the numerical fingerprints of the KT transition reported in Sec. IV A.

(1) *Scale invariance at the critical point*. First of all we estimate the critical point. We can do this by FSS of the crossing points of $U_4(T,N)$. Such estimate is, however, more and more difficult as ρ increases because the low-T behavior of $U_4(T,N)$ is less and less size dependent than the high-T behavior as N increases, as shown in Fig. 16. This appears to be a precursor of the low-T size independence occurring in 2d at the KT transition, as we already mentioned. Nevertheless we obtain $T_c = 1.62(2), 1.57(1)$, and $1.38(2)$ for $\rho = 3.75, 3.875$, and 4.667, respectively. We can, otherwise, estimate T_c by

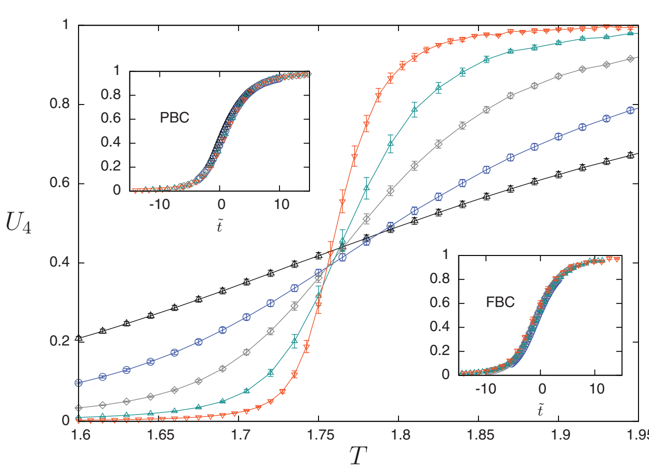

FIG. 14. (Color online) Binder cumulant versus temperature for $\rho = 10/3$ in the non-mean-field regime. The upper inset shows the scaling as in Fig. 10 with $\bar{\nu} = 2.19(2)$, while the lower inset shows the scaling in the $\rho = 10/3$ system with FBC and with $\bar{\nu} = 2.24(4)$.

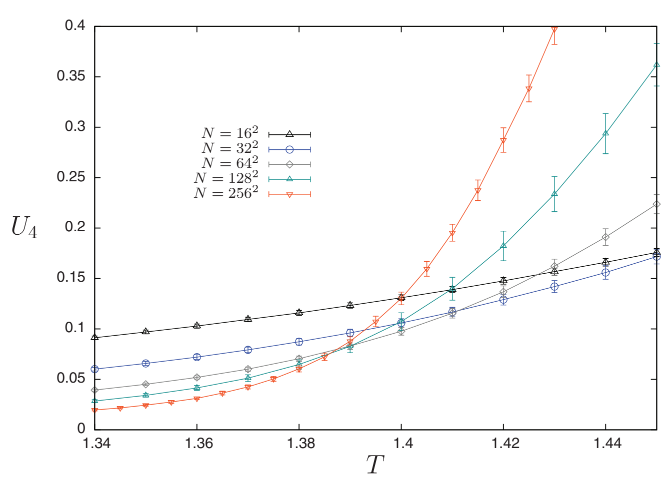

FIG. 16. (Color online) Binder cumulant versus temperature for $\rho = 4.667$ in the short-range regime. There is evidence for the scale-invariance of this quantity for $T < T_c$ in the large-N limit.

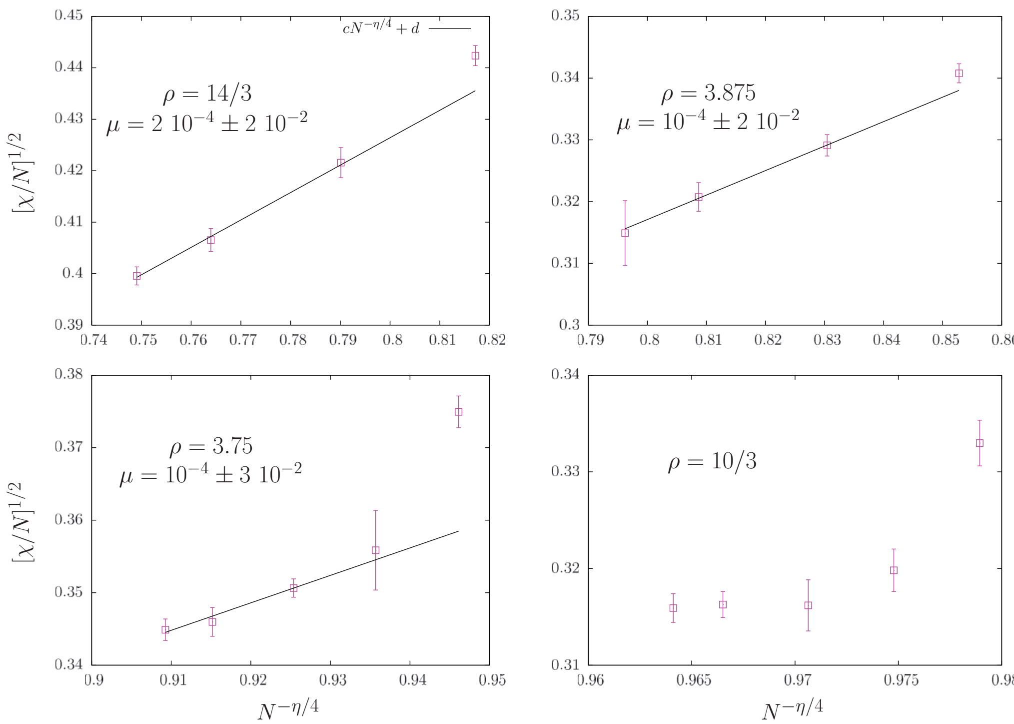

FIG. 17. (Color online) Scaling of $\sqrt{\chi/N}$ vs $N^{-\eta/4}$ at $T < T_c$ for three values of ρ in the SR regime and for $\rho = 10/3 < \rho_{\rm sr}$. The black lines are linear fits and the y-axis intercept μ is reported. For the three cases in the SR regime, the fitted value of μ is compatible with zero.

means of the fixed-U_4 FSS method, yielding $T_c = 1.63(1)$, 1,58(1), and 1.36(1), respectively. One can notice that the estimates for $\rho = 4.667$ do not coincide because of the mentioned limits of the crossings method.

(2) *Susceptibility scaling at criticality*. In the 2d XY model the susceptibility at criticality behaves like Eq. (27) with $\eta(T_c) = 1/4$.[60] We numerically interpolated Eq. (27) at different temperatures for different ρ in the candidate short-range regime and also for $\rho = 10/3 < \rho_{\rm sr}$. The behavior of $\eta(T)$ is reported in Fig. 7 for all these cases. As a reference, in the figure we also display the critical temperature intervals (vertical stripes), as estimated by the FSS method at fixed U_4. For all $\rho \geqslant 3.75$ we find that the temperature at which $\eta = 1/4$ is compatible, in the statistical error, with our estimate for T_c. This is not the case, instead, for $\rho = 10/3$. This hints that the conjectured $\rho_{\rm sr} = 3.75$ is actually the threshold between LR and SR universality classes. In terms of the SR-LR equivalence, formulated in Eq. (4), this confirms that $\rho_{\rm sr}$ is equivalent to $D = 2$.

As a further confirmation of the fact that $\rho_{\rm sr} = 3.75$, we present in Fig. 17 the behavior of the quantity $[\chi(T,N)/N]^{1/2}$ vs $N^{-\eta(T)/4}$ for four values of ρ and for T values below the critical temperature. This allows for a self-consistency test of the scaling $\chi \sim N^{1-\eta/2}$ supposed in Fig. 7. In the SR regime, this quantity should behave as $[\chi/N]^{1/2} \sim N^{-\eta/4}$ for large N. As can be seen in Fig. 17, this is verified for $\rho \geqslant 3.75$ and clearly not for $\rho = 10/3$.

Once we are convinced that for $\rho \geqslant 3.75$ the system is in the KT universality class, we can, vice versa, interpolate a value of T_c as the temperature at which $\eta(T_c) = 1/4$, yielding by a simple linear interpolation, $T_c = 1.60(2), 1.56(1)$, and $1.37(1)$ for $\rho = 3.75$, 3.875, and 4.667, respectively.

(3) *Magnetization in the low-T phase*. The behavior of the magnetization below criticality is peculiar and might not be the same for all values of ρ in the SR regime. Analytic results for XY spins on a random graph of spectral dimension $\bar{d}$,[15] indeed, prove that for $\bar{d} \leqslant 2$ the magnetization is zero in the thermodynamic limit and it is nonzero for $\bar{d} > 2$. For ρ large enough the squared magnetization goes to zero with the same scaling of the susceptibility ($\sim N^{-1/16}$); see Sec. IV A, Eq. (28). For $\rho = 4.667$, e.g., for which $\bar{d} = 2$, we plot $(\overline{\langle \mathbf{m}^2 \rangle})^{1/2}$ in Fig. 18. As ρ decreases below 4 we have $\bar{d} > 2$. This implies a nonzero asymptotic value for $\overline{\langle \mathbf{m} \rangle^2}$ as $\rho < 4$ and, thus, different

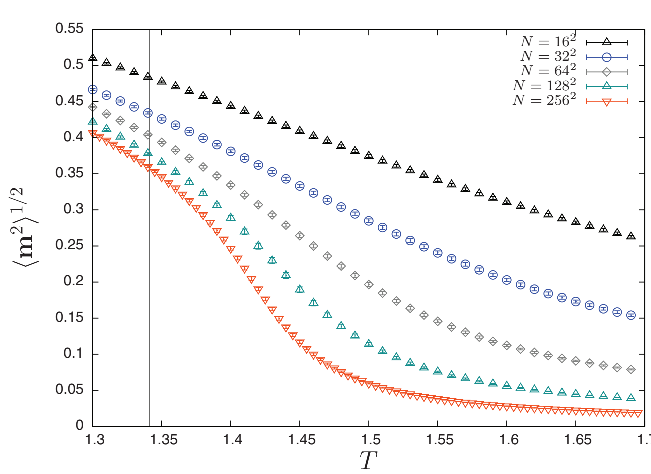

FIG. 18. (Color online) Magnetization versus temperature for $\rho = 4.667$ in the short-range regime. In the low-T phase the magnetization monotonically decreases with N.

scalings for χ and $(\overline{\langle \mathbf{m}^2 \rangle})^{1/2}$. In particular, the Lévy graph with $\rho = 3.875$ has $\bar{d} = 4/(\rho - 2) = 2.1333\ldots$ and $\rho = 3.75$ has spectral dimension $\bar{d} = 2.2857\ldots$. Unfortunately, because of the very slow scaling of the susceptibility it is rather hard to tell whether the asymptotic limit of the magnetization is compatible with a strictly positive value. As ρ is near the SR threshold $\rho = 3.75$ we can, actually, not detect any relevant discrepancy with the χ scalings reported in Fig. 17.

(4) The specific heat is not divergent nor discontinuous at the transition; cf. Fig. 11, right panel.

(5) *Kosterlitz-Thouless law*. We have estimated the critical temperature in the SR regime using Eq. (29) at different sizes and taking the FSS of the fit parameter estimates, as we did for the square lattice case in Sec. IV A. We obtain $T_c = 1.59(1)$ for $\rho = 3.875$ and $T_c = 1.34(2)$ for $\rho = 4.667$. These estimates agree with the ones obtained from the FSS of the temperature at which the system presents a given value of U_4, $T_f(U_4,N)$.

We summarize our results in all regimes in Table II.

V. CONCLUSIONS AND PERSPECTIVES

The outcome of extensive numerical simulations on the 2d Lévy lattice yield evidence for three different critical regimes, corresponding to given intervals in the Lévy exponent ρ governing the topology of the graphs: short-range $\rho \in [\rho_{\rm sr},\infty)$, non-mean-field long-range $\rho \in (\rho_{\rm mf},\rho_{\rm sr})$, and mean-field $\rho \in [0,\rho_{\rm mf}]$, with $\rho_{\rm mf} = 3$ and $\rho_{\rm sr} = 3.75$. The SR threshold value has been determined in Sec. IV E, where we found evidence that $\eta = 1/4$ for $\rho \geqslant 3.75$ from the susceptibility scaling.

Studying the spectral dimension we verified that its expression, Eq. (9), holding for fully connected long-range models still holds in the dilute case. The identification $\bar{d}(\rho) = 2d/(\rho - d)$ appears, indeed, to be confirmed by a numerical estimation; see Fig. 3 and Appendix A. Furthermore, for $\rho \to d$, $\bar{d}$ diverges. An infinite spectral dimension, indeed, occurs in the Bethe lattice limit and, generally, in any graphs not satisfying the polynomial growth condition.[54] The spectral dimension does not depend on the symmetry of the system but only on the topology of the graph.

In the mean-field regime we measured the critical exponents that we found always consistent with the mean-field values $\gamma = 1$, $\alpha = 0$, and $\bar{\nu} = 2$. The latter is the correlation volume exponent, related with the correlation length exponent that we found always consistent with their mean-field values $\nu = \bar{\nu}/D_{\rm u} = 1/2$. These exponents agree with the already mentioned theoretical predictions for the D-dimensional equivalent model in the mean-field regime: ν_ρ, η_ρ, γ_ρ (see Sec. IV C). In the long-range non-mean-field regime, instead, we find a continuous phase transition with different critical exponents and a low-temperature phase exhibiting spontaneous symmetry breaking. Finally, we report evidence for the onset of a KT-like transition in the short-range regime for $\rho \geqslant \rho_{\rm sr} = 2 + d - \eta_{\rm sr}(2) = 3.75$. In this regime we have the value $\rho = 4$ corresponding to a spectral dimension $\bar{d} = 2$. It is known[15] that the *XY* model exhibits zero magnetization in graphs with $\bar{d} = 2$ [i.e., for $\rho \geqslant 4$; see Eq. (9)], whereas for $\bar{d} > 2$ ($\rho < 4$) a finite magnetization should occur.[14] Due to the very slow FSS of the magnetization ($\sim N^{-1/16}$ if the asymptotic value is zero), however, and because of the fact that for $\rho \lesssim 4$ the asymptotic magnetization is expected to be small, we have not been able to identify a spontaneous $O(2)$ symmetry breaking for $\rho < 4$ with the simulated sizes.

For each value of ρ, the critical behavior can be conjectured to be in a one-to-one correspondence with a short-range *XY* model in D dimensions. This short-range effective dimension is exactly $D = d = 2$ for $\rho \geqslant \rho_{\rm sr}(d)$, and $D = 2d/(\rho - d)$ for $\rho \in (d,3/2d)$, cf. Eq. (3), in the mean-field regime. As $\rho \to d$, D tends to infinity. This is the value of ρ for which the fully connected version of the model displays a divergent energy.

The most delicate regime is the non-mean-field long-range one, for which Eq. (3) does not hold anymore and the dimensional relationship derived from the SR-LR equivalence hypothesis is conjectured to be given by Eq. (4). This can be derived, e.g., from a free energy scaling argument[51] or by requiring the exact match with the SR regime at $\rho_{\rm sr}$.[43] As said in Sec. I, Eq. (4) has been tested in the 1d Lévy Ising spin glass and in the 2d (fully connected) ordered Ising model. In the first case the correspondence between short-range and long-range critical behavior is actually consistent both for $D = 3$ and for $D = 4$, the compatibility improving the higher D.[51] In the Ising ferromagnet case, on the other hand, such a correspondence is consistent nearer to the mean-field threshold ($D = 2$), but for $\rho = 1.875$, for which $D = 3$, the critical exponents are no longer compatible with the 3d ones. In the 2d *XY* model, we do not observe a strong disagreement for $D(\rho) = 3$, that is, for $\rho = 3.307933$, but our more refined estimates are not compatible with the 3d results within the statistical error. Indeed, we obtain $\gamma = 1.42(7), \bar{\nu} = 2.18(2)$, and $\beta = 0.39(2)$ to be compared with the values $\gamma_{\rm 3d} = 1.3178(2)$, $\bar{\nu}_{\rm 3d} = 2.0151(3)$, and $\beta_{\rm 3d} = 0.3486(1)$ of Ref. 57. We stress that the 2d limit is quite peculiar due to the uncommon specific critical properties of the KT transition, where the low-temperature phase is unmagnetized and it is critical at all $T \leqslant T_c$ with temperature-dependent critical exponents and where χ and ξ diverge exponentially rather than with a power law and the very definition of $\bar{\nu} = \nu/2$ and γ lacks, for $\rho < \rho_{\rm sr} = 3.75$. The 3d values nevertheless seem to be not too far away from the approximated SR-LR correspondence expressed by Eqs. (4), (24), and (26).

We have further determined that the spectral dimension is related with the dimension D of a short-range lattice equivalent to the Lévy lattice for what concerns the critical behavior. The two are identical in the mean-field regime, $\rho \leqslant 3$; cf. Eq. (3) and Eq. (9). In this regime the structure of the graph alone is enough to determine the universality class of the system, independently of the symmetries of the system variables. Beyond the mean-field threshold symmetries of the specific system defined on the graph become relevant and the identification does not hold anymore until $\rho \geqslant 4$ and the graph is by all means a bi-dimensional lattice: $\bar{d} = d = 2$. The result $D = \bar{d}$, valid in the mean-filed regime, implies that the critical behavior of the $O(2)$ model on a graph characterized by a spectral dimension $\bar{d}$ coincides with the one of the short-range $\bar{d}$-dimensional $O(2)$ model, allowing for a deeper understanding of the physics of interacting systems on nonregular structures and extending the known universal properties of the spectral dimension of the $O(n \to \infty)$ model[11] to finite n.

Summarizing, we have found that the critical properties of the $O(2)$ model in a graph can be divided into three regimes characterized by the spectral dimension of the graph. In the mean-field regime it plays the role of the dimension of a short-range model with common critical properties. In the infrared divergent long-range regime $\bar{d}$ and D do not coincide but are, somewhat, related, though the conjectured relationship Eq. (3) does not seem to hold for $\rho \in [\rho_{\mathrm{mf}} : \rho_{\mathrm{sr}}]$. As a perspective, we propose to investigate how the introduction of disorder and a different short-range kind of criticality would change this scenario.[53] This is the object of ongoing research.

ACKNOWLEDGMENTS

We acknowledge Raffaella Burioni, Martin Hasenbusch, and Flaviano Moroni for very interesting discussions. We thank the QUonG initiative of the INFN APE group for the use of their GPU cluster. The research leading to these results has received funding from the Italian Ministry of Education, University, and Research under the Basic Research Investigation Fund (FIRB/2008) program/CINECA, Grant Code RBFR08M3P4, and under the PRIN2010 program, Grant Code 2010HXAW77-008, and from the People Programme (Marie Curie Actions) of the European Union's Seventh Framework Programme FP7/2007-2013 under REA Grant Agreement No. 290038, NETADIS project.

APPENDIX A: SPECTRAL DENSITY ESTIMATION

In order to estimate $\bar{d}$ we have studied the histogram of return times of a collectivity of 4×10^4 random walkers averaging over 20 different finite-size realizations of 2d dilute graphs with power $\rho = \infty$, 5, 4.5, 4, 3.8, 11/3, and 10/3. We have performed random walks on lattices of size $N = 128^2$, 196^2, 512^2 and, for the smallest value of ρ, $N = 768^2$. We have taken average coordination numbers $z = 4$ and, for a comparison, $z = 8$. Changing the average connectivity of the sites does not change the spectral dimension, within the statistical errors, at any given size. Finite-size effects are there, instead, as ρ decreases, as discussed in Sec. II B.

The histogram of return times is proportional to the probability of self-return of a random walker in the graph after a time τ: $P(\tau)$. For large values of $\rho > 2 + d$ and in the square lattice case the estimation of $\bar{d}$ is very accurate since the function P presents a very clear power-law behavior even at large times and finite-size effects are not an issue. For smaller values of ρ, however, such a measure becomes less and less accurate. This is due to the presence of "shortcuts" on the graph that take the walker to the boundaries of the original lattice, where the probability P is overestimated, and to the existence of low-connected nodes. To cope with these drawbacks, for $\rho > 4$ our random walkers start from the center of the original finite-size 2d lattice, while for $\rho \leqslant 4$, each realization of the walker starts from a node which is chosen at random between the subset of nodes whose degree is larger than two. In Fig. 19 we present the P histograms (up to an arbitrary, ρ-dependent constant) for each studied value of ρ, from which the data of Fig. 3 have been inferred.

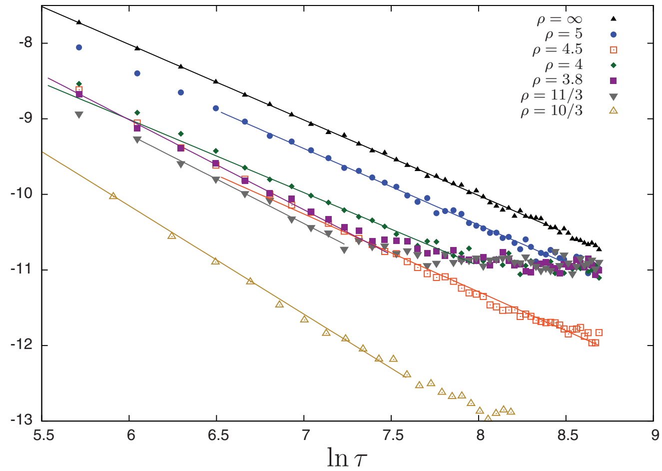

FIG. 19. (Color online) Logarithm of the histogram of self-return times of a random walker in dilute 2d graphs of size $N = 196^2$ with different values of ρ. Points are the numerical measures, while lines are the fits with a linear function (their end points indicate the corresponding fit intervals). The slope of the fits is $-1/2$ times the spectral dimension (see Fig. 3).

APPENDIX B: DETAILS OF THE ALGORITHM

We present here a detailed description of the algorithm used: a home-made high-performance parallel code for the Monte Carlo dynamics of spin models defined on general networks. The software is developed for GPU architecture and it has been developed with the CUDA programming model. A single-spin-flip Metropolis update has been used, with nonconnected spins being updated in parallel by different GPU cores. Though this might not be the optimal algorithm for the specific case of the long-range ferromagnet, the kind of parallel programming we propose has rather competitive performances and, on top of that, is straightforwardly exportable to any kind of system with continuous variables, including models with random bonds and fields.

1. Graph coloring

This procedure requires the *coloring* of each realization of the randomly generated graph before dynamics starts. The graph nodes are colored with the same color if they are not connected to each other. During the simulation, sites with a common color are Metropolis-updated synchronously, and subsets of the set of vertexes corresponding to different colors are processed sequentially on each MCS. This is a generalization of the so called red-black Gauss-Seidel algorithm used in the parallelization of spin operations in bipartite graphs, such as hypercubic lattices.

We approximately color the graph using a variant of the smallest-last-ordering (SLO) algorithm,[63,64] costing $O(N)$. For the simulated sizes ($N \leqslant 2^{16}$) the number of colors (equal to 2 in the $\rho = \infty$ case) turns out to be never larger than 6. As one can see in Fig. 20, with our coloring procedure the distribution of noninteracting sets becomes more and more homogeneous as N increases, thus automatically enhancing the algorithm efficiency.[64]

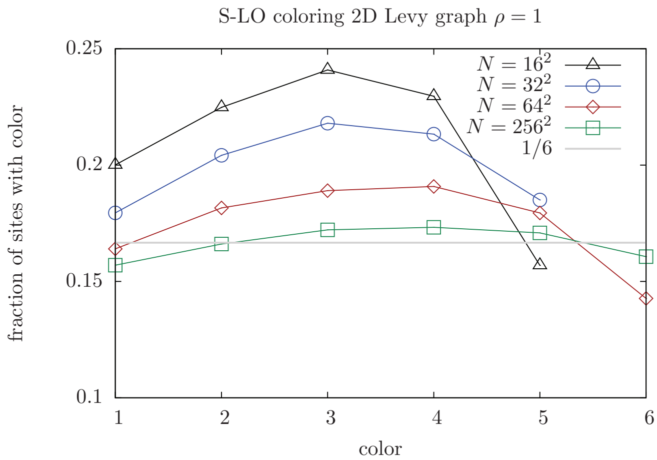

FIG. 20. (Color online) Coloring a dilute Lévy 2d graph with power $\rho = 1$ and $N = L^2 = 2^{8-14}$ nodes with the SLO algorithm. The larger the graph, the more homogeneous is the partition of the set of graph nodes in subsets corresponding to different colors.

2. Improved equilibrium dynamics

In our code, besides the Metropolis algorithm, also the parallel tempering (PT)[65] and overrelaxation (OR)[66] algorithms are implemented. Both algorithms reduce the correlation time of the Monte Carlo Markov processes and improve the equilibration.[77]

PT swap attempts are performed (in CPU) every MCS, with replicas at different temperatures being updated in parallel, as explained in Ref. 67. Figure 21 illustrates the rate of PT swaps between configurations with adjacent temperatures at fixed intervals of $\Delta T = 0.005$, as a function of the temperature for a system with $N = 2^{16}$ in the 2d square lattice, for which the critical temperature is known to be $Tc = 0.8929\ldots$.

3. Memory management

We have used a storage of the degrees of freedom in the *global device memory* of the GPU architecture,[67,68] each *thread* accessing the $O(2)$ angle of its corresponding graph node in such a way that sites with a common color are consecutive in the array, favoring *coalesced* memory access. Each *thread*, then, accesses an array in global memory, from which it reads the list of sites connected to the corresponding site. An independent random number generator of the Fibonacci type[67] is associated to each *device thread*. We used double floating-point precision for storing observables, and single precision for the calculation of the trigonometric functions in the evaluation of the energy and magnetization of each site. In the latter case we adopted the special $\mathsf{fast}_{\mathsf{math}}$ function of the GPU architecture, a faster routine specific of the GPU architecture.

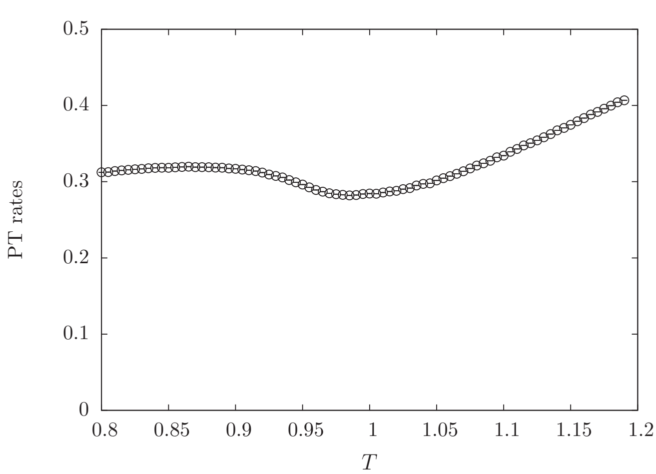

FIG. 21. Exchange rate between nearby heat baths in the PT algorithm in a square lattice with $N = 2^{16}$ sites. The distance between consecutive temperatures is $\Delta T = 0.005$.

TABLE III. Computational time of different algorithms per spin. It is the total computation time of a run divided by N, by the number of copies N_T at different temperatures in the PT algorithm, and by the number of MCSs.

Algorithm	Precision	Trig. function	Time per spin (ns)
MET + PT	single	fast	1.88
MET	single	fast	0.635
MET	single	cosf	0.865
OR	single	fast	0.36
OR	single	cosf	0.54

4. Computational speed

We now present some details about the performance of our algorithm, referring to a calculation performed in an nVidia GPU GTX480 Fermi card. In Table III the reader may find the computation time per spin involved in the Metropolis and OR algorithms in a square lattice with $N = 2^{14}$ sites and PBC, for different choices of the floating point precision and of the routine used for the computation of trigonometric operations. In Fig. 22 a comparison of the computation time for the PBC square and Lévy lattice with $\rho = 7/3$ with different sizes is shown. Since in a general graph colored with Q colors our algorithm is nearly $Q/2$ times slower than the code in the square lattice, we also show $2/Q$ times the computation time

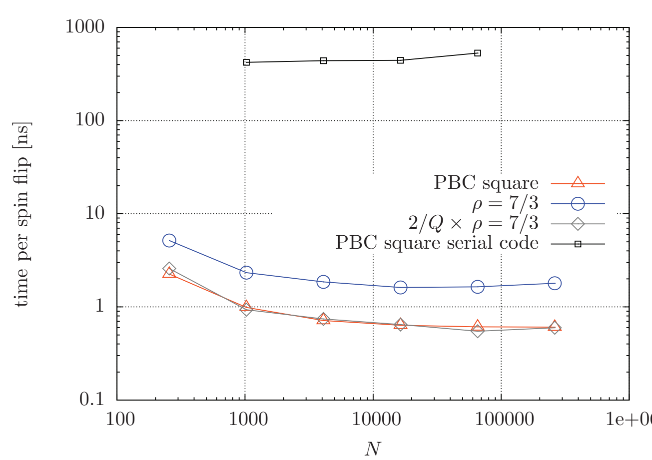

FIG. 22. (Color online) Computational time per spin of the Metropolis algorithm versus N for the square nearest-neighbor lattice and $\rho = 7/3$ Lévy lattice. The serial-CPU run is shown for comparison: a speedup of several hundreds of times can be observed.

in the Lévy graph for comparison with the square lattice case. The minimum time peaks for Metropolis and OR algorithms are 0.55 ns and 0.36 ns respectively, a mark which is competitive with state-of-the-art highly optimized GPU simulations of spin glasses[69] [a direct comparison is not possible since their benchmark refers to the $O(3)$ model] and represents a speedup of several hundred times with respect to a serial C code running on an Intel i7 CPU with 2.67 GHz. All of the simulations in this work have been performed using single precision (4 bytes) for the storing of floating-point numbers and the fast_math CUDA functions. We ran simulations changing both precision and trigonometric routines, and introducing OR sweeps, without finding essential accuracy improvements. An upgraded and generalized version of this algorithm, designed for the study of random laser modes[70–73] in arbitrary topologies, will be extensively reviewed and presented in a forthcoming work.[64]

APPENDIX C: FINITE-SIZE SCALING ANALYSIS OF CRITICAL PARAMETERS

Critical temperature. For each value of ρ, we have estimated T_c both from the FSS of the crossing points of U_4 at different sizes (see, e.g, Figs. 10, 14) and from the FSS of the temperature at which a finite-size system exhibits a given value U_4 of the Binder cumulant:

$$T_f(U_4,N) = T_c + A\,N^{-x}, \tag{C1}$$

$T_c = T_f(U_4,\infty)$ being the critical temperature, independent from the specific U_4 value chosen for the fit, and x, a quantity in principle depending on U_4, and that can be identified with $1/\bar{\nu}$ for $\rho < 3.75$ (cf. Fig. 4). In order to find T_c, (i) we take different values of the Binder cumulant $U_4^{(j)}$, $j = 1\ldots n_d$, in a reasonable range around the critical region; (ii) we construct n_d apart data sets $\{T_f(U_4^{(j)},N)\}_j$; and (iii) we interpolate all data sets simultaneously with common parameter T_c and set-depending parameters $A(j)$, $x(j)$. The resulting temperatures are reported in Table II and plotted in Fig. 4 together with the T_c estimated from the FSS of the crossing points. In practice, for $\rho < \rho_{\rm sr} = 3.75$, we fix x to be common to all U_4 values, while for $\rho > 3.75$ it is U_4 dependent.

Correlation volume exponent. Besides estimating $\bar{\nu}$ from the interpolation with Eq. (C1), in order to have a more precise determination we estimated the correlation volume exponent from the logarithm of the temperature derivative of the binder $\dot{U}_4(T,N)$ at fixed U_4, performing a simultaneous FSS fit over apart data sets at different values of the Binder cumulant with the law

$$\ln \dot{U}_4(T_j,N) = c_j + \frac{1}{\bar{\nu}}\,\ln N \tag{C2}$$

and with a common value of $\bar{\nu}$ for all data sets. We obtain the results plotted in Fig. 5 and reported in Table II.

Susceptibility exponent. The $\gamma/\bar{\nu}$ exponent has been determined from the FSS (21) in the approximated form

$$\ln \chi(T,N) = \mathrm{cte}(T) + x(T)\ln N \tag{C3}$$

where $x(T_c)$ can be identified with $\gamma/\bar{\nu}$ in the MF, LR regimes, and $x(T)$ can be identified with $1-\eta(T)/2$ in the SR regime, when $T \leqslant T_c$. We have interpolated $x(T)$ for several values of the temperature in the scaling region, (as shown in Fig. 7), and estimated the values of $\gamma/\bar{\nu}$ from the values of $x(T)$ with T in the error interval of T_c, estimated as explained above. Finally, γ is obtained by multiplying the interpolated $\gamma/\bar{\nu}$ by the $\bar{\nu}$ obtained from the U_4 fit. The resulting values of γ and of $\gamma/\bar{\nu}$ so computed are shown in Fig. 6.

Magnetization exponent β. The exponent β is estimated in a similar way as done for the γ in Eq. (C3), assuming the FSS:

$$\tfrac{1}{2}\ln \overline{\langle \mathbf{m}^2\rangle}(T,N) = \mathrm{cte}(T) - x(T)\ln N, \quad T<0; \tag{C4}$$

identifying $x(T_c)$ with $\beta/\bar{\nu}$ yields the estimates reported in Table II. It is interesting to remark that the (Rushbrooke-Widom) scaling relation between critical exponents $\gamma/\bar{\nu} = 1 - 2\beta/\bar{\nu}$ is satisfied. The quantity $1-2\beta/\bar{\nu}$ is reported in Fig. 6 for several values of ρ, illustrating the validity of the Rushbrooke-Widom relation.

*miguel.berganza@roma1.infn.it
†luca.leuzzi@cnr.it

[1] A. Krawiecki, J. A. Hołyst, and D. Helbing, Phys. Rev. Lett. **89**, 158701 (2002).
[2] J.-S. Yang, S. Chae, W.-S. Jung, and H.-T. Moon, Physica A **363**, 377 (2006).
[3] J.-S. Yang, W. Kwak, T. Kaizoji, and I.-m. Kim, Eur. Phys. J. B **61**, 241 (2008).
[4] J. S. Yang, W. Kwak, G. Kwang-Il, and I. Kim, Europhys. Lett. **84**, 36004 (2008).
[5] W. Bialek, A. Cavagna, I. Giardina, T. Mora, E. Silvestri, M. Viale, and A. M. Walczak, Proc. Natl. Acad. Sci. USA **109**, 4786 (2012).
[6] L. de Arcangelis and H. J. Herrmann, Proc. Natl. Acad. Sci. USA **107**, 3977 (2010).
[7] D. De Martino, M. Figliuzzi, A. De Martino, and E. Marinari, PLoS Comput. Biol. **8**, e1002562 (2012).
[8] A. De Martino, D. De Martino, R. Mult, and G. Uguzzoni, PLoS One **7**, e39849 (2012).
[9] S. N. Dorogovtsev, A. V. Goltsev, and J. F. F. Mendes, Rev. Mod. Phys. **80**, 1275 (2008).
[10] H. E. Stanley, Phys. Rev. **176**, 718 (1968).
[11] R. Burioni, D. Cassi, and C. Destri, Phys. Rev. Lett. **85**, 1496 (2000).
[12] D. Cassi and L. Fabbian, J. Phys. A **32**, L93 (1999).
[13] K. Hattori, T. Hattori, and H. Watanabe, Prog. Theor. Phys. Suppl. **92**, 108 (1987).
[14] R. Burioni, D. Cassi, and A. Vezzani, Phys. Rev. E **60**, 1500 (1999).
[15] D. Cassi, Phys. Rev. Lett. **68**, 3631 (1992).
[16] J. M. Kosterlitz and D. J. Thouless, J. Phys. C **6**, 1181 (1973).
[17] J. M. Kosterlitz, J. Phys. C **7**, 1046 (1974).
[18] N. D. Mermin and H. Wagner, Phys. Rev. Lett. **17**, 1133 (1966).
[19] A. Barrat and M. Weigt, Eur. Phys. J. B **13**, 547 (2000).
[20] M. Gitterman, J. Phys. A **33**, 8373 (2000).
[21] C. P. Herrero, Phys. Rev. E **65**, 066110 (2002).

[22]H. Hong, B. J. Kim, and M. Y. Choi, Phys. Rev. E **66**, 018101 (2002).
[23]W. Kwak, J. S. Yang, J. I. Sohn, and I. M. Kim, Phys. Rev. E **75**, 061130 (2007).
[24]G. Bianconi, Phys. Lett. A **303**, 166 (2002).
[25]A. Aleksiejuk, J. A. Hoyst, and D. Stauffer, Physica A **310**, 260 (2002).
[26]M. Leone, A. Vazquez, A. Vespignani, and R. Zecchina, Eur. Phys. J. B **28**, 191 (2002).
[27]S. N. Dorogovtsev, A. V. Goltsev, and J. F. F. Mendes, Phys. Rev. E **66**, 016104 (2002).
[28]C. P. Herrero, Phys. Rev. E **69**, 067109 (2004).
[29]M. Bauer, S. Coulomb, and S. N. Dorogovtsev, Phys. Rev. Lett. **94**, 200602 (2005).
[30]D. S. Callaway, J. E. Hopcroft, J. M. Kleinberg, M. E. J. Newman, and S. H. Strogatz, Phys. Rev. E **64**, 041902 (2001).
[31]S. N. Dorogovtsev, Phys. Rev. E **67**, 045102 (2003).
[32]F. Iglói and L. Turban, Phys. Rev. E **66**, 036140 (2002).
[33]S. N. Dorogovtsev, A. V. Goltsev, and J. F. F. Mendes, Eur. Phys. J. B **38**, 177 (2004).
[34]E. Khajeh, S. N. Dorogovtsev, and J. F. F. Mendes, Phys. Rev. E **75**, 041112 (2007).
[35]B. J. Kim, H. Hong, P. Holme, G. S. Jeon, P. Minnhagen, and M. Y. Choi, Phys. Rev. E **64**, 056135 (2001).
[36]J.-S. Yang, K.-I. Goh, I.-m. Kim, and W. Kwak, New J. Phys. **11**, 063048 (2009).
[37]L. Leuzzi, G. Parisi, F. Ricci-Tersenghi, and J. J. Ruiz-Lorenzo, Phys. Rev. Lett. **101**, 107203 (2008).
[38]L. Leuzzi, G. Parisi, F. Ricci-Tersenghi, and J. J. Ruiz-Lorenzo, Philos. Mag. **91**, 1917 (2011).
[39]L. Leuzzi, G. Parisi, F. Ricci-Tersenghi, and J. J. Ruiz-Lorenzo, Phys. Rev. Lett. **103**, 267201 (2009).
[40]H. G. Katzgraber, D. Larson, and A. P. Young, Phys. Rev. Lett. **102**, 177205 (2009).
[41]A. Sharma and A. P. Young, Phys. Rev. B **84**, 014428 (2011).
[42]D. Larson, H. G. Katzgraber, M. A. Moore, and A. P. Young, Phys. Rev. B **81**, 064415 (2010).
[43]L. Leuzzi and G. Parisi, arXiv:1303.6333.
[44]D. X. Viet and H. Kawamura, Phys. Rev. Lett. **105**, 097206 (2010).
[45]A. Sharma and A. P. Young, Phys. Rev. B **83**, 214405 (2011).
[46]F. Beyer, M. Weigel, and M. A. Moore, Phys. Rev. B **86**, 014431 (2012).
[47]M. E. Fisher, S. K. Ma, and B. G. Nickel, Phys. Rev. Lett. **29**, 917 (1972).
[48]G. Kotliar, P. W. Anderson, and D. L. Stein, Phys. Rev. B **27**, 602 (1983).
[49]L. Leuzzi, J. Phys. A **32**, 1417 (1999).
[50]M. Picco, arXiv:1207.1018.
[51]R. A. Baños, L. A. Fernández, V. Martín-Mayor, and A. P. Young, Phys. Rev. B **86**, 134416 (2012).
[52]M. C. Angelini, Ph.D. thesis, Università di Roma, 2012, http://server2.phys.uniroma1.it/DipWeb/dottorato/DOTT_FISICA/MENU/03DOTTORANDI/TesiFin25/Angelini.pdf.
[53]R. Burioni and D. Cassi, Mod. Phys. Lett. B **11**, 1095 (1997).
[54]R. Burioni and D. Cassi, J. Phys. A **38**, R45 (2005).
[55]D. J. Amit and V. Martín-Mayor, *Field Theory, the Renormalization Group, and Critical Phenomena* (World Scientific, Singapore, 2005).
[56]R. Botet, R. Jullien, and P. Pfeuty, Phys. Rev. Lett. **49**, 478 (1982).
[57]M. Campostrini, M. Hasenbusch, A. Pelissetto, and E. Vicari, Phys. Rev. B **74**, 144506 (2006).
[58]R. Gupta, J. DeLapp, G. G. Batrouni, G. C. Fox, C. F. Baillie, and J. Apostolakis, Phys. Rev. Lett. **61**, 1996 (1988).
[59]H. G. Ballesteros, A. Cruz, L. A. Fernández, V. Martín-Mayor, J. Pech, J. J. Ruiz-Lorenzo, A. Tarancón, P. Téllez, C. L. Ullod, and C. Ungil, Phys. Rev. B **62**, 14237 (2000).
[60]D. J. Amit, Y. Y. Goldschmidt, and S. Grinstein, J. Phys. A **13**, 585 (1980).
[61]M. Hasenbusch, J. Phys. A **38**, 5869 (2005).
[62]F. Morone and F. Ricci-Tersenghi (private communication).
[63]D. W. Matula and L. L. Beck, J. Assoc. Comput. Mach. **30**, 417 (1983).
[64]M. I. Berganza and L. Leuzzi (unpublished).
[65]K. Hukushima and K. Nemoto, J. Phys. Soc. Jpn. **65**, 1604 (1996).
[66]M. Creutz, Phys. Rev. D **36**, 515 (1987).
[67]M. Weigel, J. Comput. Phys. **231**, 3064 (2012).
[68]E. E. Ferrero, J. P. De Francesco, N. Wolovick, and S. A. Cannas, Comput. Phys. Commun. **183**, 1578 (2012).
[69]T. Yavors'kii and M. Weigel, Eur. Phys. J. Spec. Top. **210**, 159 (2012).
[70]H. Cao, Waves Random Media **13**, R1 (2003).
[71]D. S. Wiersma, Nat. Phys. **4**, 359 (2008).
[72]L. Leuzzi, C. Conti, V. Folli, L. Angelani, and G. Ruocco, Phys. Rev. Lett. **102**, 083901 (2009).
[73]C. Conti and L. Leuzzi, Phys. Rev. B **83**, 134204 (2011).
[74]U. Wolf, Phys. Lett. B **288**, 166 (1992).
[75]E. Luijten and H. W. J. Blöte, Int. J. Mod. Phys. C **6**, 359 (1995).
[76]E. Luijten and H. W. J. Blöte, Phys. Rev. Lett. **76**, 1557 (1996).
[77]An alternative optimization can be realized by adopting cluster accelerating algorithms adapted to dilute long-range systems; see, e.g., Refs. 74–76. We do not implement such algorithms in the present work.